A Damage Sensor Associated with the Cuticle Coordinates Three Core Environmental Stress Responses in Caenorhabditis elegans

William Dodd, Lanlan Tang, Jean-Christophe Lone, Keon Wimberly, Cheng-Wei Wu, Claudia Consalvo, Joni Wright, Nathalie Pujol, Keith Choe

Genetics: Early Online, published on February 27, 2018 as 10.1534/genetics.118.300827

A damage sensor associated with the cuticle coordinates three core environmental stress responses in *C. elegans*

William Dodd[1]*, Lanlan Tang[1]*, Jean-Christophe Lone[2], Keon Wimberly[1], Cheng-Wei Wu[1], Claudia Consalvo[1], Joni E. Wright[1], Nathalie Pujol[2†] and Keith P. Choe[1†]

[1]Department of Biology, University of Florida, Gainesville, FL 32611
[2]Aix Marseille Univ, CNRS, INSERM, CIML, Marseille, France
*co-first authors; †Corresponding authors

Contact: kchoe@ufl.edu; pujol@ciml.univ-mrs.fr

Running title: Matrix regulation of stress responses

ABSTRACT

Extracellular matrix barriers and inducible cytoprotective genes form successive lines of defense against chemical and microbial environmental stressors. The barrier in nematodes is a collagenous extracellular matrix called the cuticle. In *C. elegans*, disruption of some cuticle collagen genes activates osmolyte and antimicrobial response genes. Physical damage to the epidermis also activates antimicrobial responses. Here, we assayed the effect of knocking down genes required for cuticle and epidermal integrity on diverse cellular stress responses. We found that disruption of specific bands of collagen, called annular furrows, co-activates detoxification, hyperosmotic, and antimicrobial response genes, but not other stress responses. Disruption of other cuticle structures and epidermal integrity does not have the same effect. Several transcription factors act downstream of furrow loss. SKN-1/Nrf and ELT-3/GATA are required for detoxification, SKN-1/Nrf is partially required for the osmolyte response, and STA-2/Stat and ELT-3/GATA for antimicrobial gene expression. Our results are consistent with a cuticle-associated damage sensor that coordinates detoxification, hyperosmotic, and antimicrobial responses through overlapping, but distinct downstream signaling.

SUMMARY

Although extracellular matrices function as protective barriers to many types of environmental insult, their role in sensing stress and regulating adaptive gene induction responses has not been studied carefully. Here, we identify a specific structural feature in the collagenous extracellular cuticle of the nematode *C. elegans* as a regulator of conserved transcription responses to oxidative, osmotic, and pathogenic stressors and explore downstream transcription factor requirements. Our results are consistent with the presence of an extracellular sensor for damage that regulates three distinct stress-inducible responses in the nuclei of epidermal cells.

KEYWORDS

Damage sensor; collagen; detoxification; osmotic stress; antimicrobial response

INTRODUCTION

Extracellular matrices (ECMs) are ubiquitous features of animal tissues composed of secreted fibrous proteins and polysaccharides. Although they were once considered inert mechanical scaffolds (HAY 1981), it is now clear that there is dynamic and reciprocal cross-talk between cells and ECMs that regulates cell differentiation, morphogenesis, and tumorigenesis (ROZARIO AND DESIMONE 2010; CLAUSE AND BARKER 2013; SAMARAKOON *et al.* 2013; WINOGRAD-KATZ *et al.* 2014; GAGGAR AND WEATHINGTON 2016). Less is known about how ECMs influence cellular responses to environmental stress.

Internal and epidermal tissues secrete ECMs as mechanical support. Epidermal ECMs also function as barriers to environmental stress. Examples include a keratin- and lipid-rich matrix in mammals (i.e., stratum corneum of the skin) and a rigid chitinous exoskeleton in insects. Nematodes such as *Caenorhabditis elegans* are covered by a flexible cuticle of cross-linked collagen fibers that is secreted by underlying epidermal cells (PAGE AND JOHNSTONE 2007; CHISHOLM AND XU 2012). It provides a first line of defense against desiccation, as well as some pathogens and toxins (ALVAREZ *et al.* 2007; PARTRIDGE *et al.* 2008; BURNS *et al.* 2010).

C. elegans mounts distinct cellular responses to stress that are broadly conserved (LAMITINA *et al.* 2006;

WHEELER AND THOMAS 2006; PUJOL *et al.* 2008a; PUJOL *et al.* 2008b; ROHLFING *et al.* 2011; CHOE 2013; ZUGASTI *et al.* 2014). In response to high osmolarity, *C. elegans* synthesizes the organic osmolyte glycerol in part by inducing *gpdh-1,* which encodes the rate-limiting enzyme GPDH (glycerol-3-phosphate dehydrogenase) (LAMITINA *et al.* 2004; LAMITINA *et al.* 2006). High osmolarity and infection with fungal pathogens that pierce the *C. elegans* cuticle induce several antimicrobial peptide genes including *nlp-29* (PUJOL *et al.* 2008a; PUJOL *et al.* 2008b; ZUGASTI *et al.* 2014). Genetic studies have identified cuticle collagens that are required to regulate *gpdh-1* and *nlp-29* under basal conditions (LAMITINA *et al.* 2006; WHEELER AND THOMAS 2006; PUJOL *et al.* 2008b; CHOE 2013; ZUGASTI *et al.* 2016) suggesting that the cuticle may contain a sensor for stress (LAMITINA *et al.* 2006; WHEELER AND THOMAS 2006; CHOE 2013; TAFFONI AND PUJOL 2015). The nature of this putative sensor and downstream signaling mechanisms remain poorly defined and it is unclear if other stress responses are also activated.

In response to reactive small molecules, cap 'n' collar (CNC) transcription factors activate antioxidant and detoxification genes in nematodes, insects, and mammals (HU *et al.* 2006; OLIVEIRA *et al.* 2009; PARK *et al.* 2009; SYKIOTIS AND BOHMANN 2010; CHOE *et al.* 2012; BLACKWELL *et al.* 2015). The single *C. elegans* CNC, SKN-1, promotes stress resistance, slows aging, and extends lifespan, while the mammalian CNC Nrf2 protects against cancer, neurodegeneration, inflammation, and fibrosis (OLIVEIRA *et al.* 2009; PARK *et al.* 2009; SYKIOTIS AND BOHMANN 2010). CNCs are regulated by a complex set of intracellular signals that influence post-translational modifications, degradation, and nuclear translocation (BRYAN *et al.* 2013; NITURE *et al.* 2013; BLACKWELL *et al.* 2015); regulation of CNCs *via* the ECM would represent a distinct mechanism.

We used RNAi to test disruption of diverse aspects of cuticle and epidermal integrity for activation of six conserved stress responses. Our results show that osmolyte accumulation and detoxification responses are co-activated by disruption of a specific cuticle structure called the annular furrow, and not by general changes in body shape or epidermal integrity. Antimicrobial response genes were also activated by furrow disruption, and more generally by loss of epidermal integrity. Hyperosmolarity also induces *skn-1* dependent detoxification genes. Surprisingly, we also find that in furrow mutants, *skn-1* is required for full induction of genes that regulate accumulation of osmolytes. Alternatively, activation of antimicrobial genes by furrow loss is dependent on STA-2/STAT and ELT-3/GATA transcription factors. Our results are consistent with the presence of a damage sensor residing in, or associated with, furrows in the cuticle that co-regulates three different stress defense pathways.

MATERIALS AND METHODS

C. elegans strains

The following strains were used: wild-type N2 Bristol, VP596 *vsIs33[dop-3p:: DsRed2];dvIs19[gst-4p::GFP]*, VP604 *kbIs24[gpdh-1p::DsRed2;myo-2p::GFP;unc-119 rescue]*, SJ4005 *zcIS4[hsp-4p::GFP]*, SJ4100 *zcIs13[hsp-6p::GFP]*, QV65 *gpls1[hsp-16.2p::GFP];vsIs33[dop-3p:: DsRed2]*, QV285 *frIs7[nlp-29p::GFP, col-12p::DsRed]*, IG274 *frIs7*, CB128 *dpy-10(e128)*, CB88 *dpy-7(e88)*, BE3 *sqt-2(sc3)*, CB61 *dpy-5(e61)*, QV41 *dpy-10(e128);vsIs33;dvIs19*, QV248 *dpy-7(e88);dvIs19*, QV261 *dpy-7(e88);kbIs24*, IG1689 *dpy-7(e88);frIs7*, IG1710 *dpy-7(e88);elt-3(gk121);frIs7*, IG1705 *dpy-7(e88);sta-2(ok1860);frIs7*, IG1685 *dpy-3(e27);frIs7*, G1709 *dpy-3(e27)elt-3(gk121);frIs7*, IG1704 *dpy-3(e27);sta-2(ok1860);frIs7*, IG1457 *dpy-10(e128);frIs7*, IG1712 *dpy-10(e128);elt-3(gk121);frIs7*, IG1707 *dpy-10(e128);sta-2(ok1860);frIs7*, TP12 *kaIs12[COL-19::GFP]*, VP332 *gpdh-1(kb24);gpdh-2(kb33)*, LD001 *ldIs7[skn-1B/C::GFP + pRF4(rol-6(su1006))]*, and GR2245 *skn-1(mg570)*. QV251, which contains a reporter for *gst-10p*, was generated using PCR to fuse 951 bp upstream from the start codon to GFP (HOBERT 2002). The fusion PCR product was then injected at approximately 20 ng/µl with *myo-3p::dsRed* as a co-marker. Unless noted otherwise, worms were cultured at 20°C using standard methods (BRENNER 1974).

RNAi and screening

RNA interference was performed by feeding worms strains of *E. coli* [HT115(DE3)] that are engineered to transcribe double stranded RNA (dsRNA) homologous to a target gene (KAMATH *et al.* 2001). The cuticle and epidermal screen in Figure 1A was performed with dsRNA feeding constructs from the ORFeome library (Open Biosystems, Huntsville, AL) (RUAL *et al.* 2004) and supplemented with clones for *dpy-10, dpy-20, dpy-3,* and *mua-6* from the genomic library (Geneservice, Cambridge, UK) (KAMATH *et al.* 2003). All clones used in Figure 1B were derived from the genomic library. Positive hit clone inserts were verified by sequencing and targets identified using Clone Mapper (THAKUR *et al.* 2014). Bacteria with plasmid pPD129.36 expressing 202 bases of dsRNA that are not homologous to any predicted *C. elegans* gene and the *sta-1(RNAi)* clone (ZUGASTI *et al.* 2016) were used as controls for non-specific RNAi effects. RNAi was performed as described previously (CHOE *et al.* 2009) with minor modifications. dsRNA producing

bacteria were grown in lysogeny broth containing selective antibiotic and then transferred to agar nematode growth medium (NGM) plates containing 0.2% □-lactose or 1 or 3 mM IPTG (CHOE *et al.* 2009). Eggs or synchronized populations of L1 larvae were placed on RNAi plates and tested at the young and gravid adult stages.

For the screen in Figure 1A, each dsRNA clone was tested with all six stress-response reporter strains in 12-well agar plates in three independent trials. Fluorescent reporter induction was scored manually as an estimate of percent penetrance (0 - similar to control vector, 1 – approximately 5-25%, 2 – approximately 25-75%, and 3 – approximately 75% or more) and averaged together across trials for each reporter strain. The penetrance of phenotypes affecting body morphology and behavior was scored on a scale of 0 to 3 (0 - similar to control vector, 1 – approximately 5-10%, 2 – approximately 10-50%, 3 – approximately 50-100%) and averaged together across all trials with all reporter strains. In all trials except the first, Dumpy was also scored for expressivity (0 – similar to control vector, 1 – mild, 2 – moderate, and 3 strong Dumpy) and the penetrance and expressivity scores were averaged together to calculate an average value for the strength of the morphology phenotype. Only results for clones that caused an average morphology phenotype score of at least 1.0 are shown.

Quantitative PCR and transgene analysis

Detoxification gene reporters (*gst-4p::GFP* and *gst-10p::GFP*) and COL-19::GFP were imaged with an Olympus BX60 microscope with UPlanFl objectives and a Zeiss Axiocam MRm camera. Fluorescence of *nlp-29p::GFP* was quantified using a COPAS BIOSORT as previously described (PUJOL *et al.* 2008a) and normalized to time of flight (TOF). The BIOSORT was not sensitive enough to reliably measure *gst-4p::GFP* and *gpdh-1p::dsRed2* fluorescence in *dpy-7* worms and these were instead quantified manually in individual worms from images using Image J 1.48v to calculate average whole-worm fluorescence. Hypodermal specific *gst-4p::GFP* fluorescence was also scored manually in individual worms as follows: low (dim signal limited to a few spots), medium (dim signal throughout the epidermis or bright signal only in head or tails regions), and high (bright signal throughout the epidermis). In one experiment, *gst-4p::GFP* was quantified using a fluorescent plate reader (Synergy HT, BioTek) (LEUNG *et al.* 2011). SKN-1b/c::GFP was visualized with a Zeiss Axiovert 200M inverted microscope and an LCM 5 Pascal Vario One confocal laser scanning system and 40x C-apochromat water objective.

Quantitative PCR assays were performed by isolating total RNA with a Quick-RNA MicroPrep kit from ZYMO Research. Reverse transcription and PCR were performed with the GoTaq 2-Step RT-qPCR system from Promega in an Eppendorf RealPlex2 using primers for *rpl-2* or *cdc-42* as internal controls. Relative mRNA levels were calculated using the delta-delta CT method adjusted with primer efficiencies calculated from standard curves. Primer sequences are in Table S1.

Whole transcriptome RNA sequencing

N2 worms were synchronized at the L1 larval stage *via* hypochlorite treatment and grown on RNAi bacteria. For high NaCl, N2 worms were transferred to 300 mM NaCl NGM agar plates as young adults and exposed for 3 or 24 hours. Mutant *dpy-7* worms were harvested one day after first becoming gravid, which corresponds to when osmotic and detoxification gene reporters are most active. RNA was extracted from three replicates per treatment, with ~1,000-2,000 worms per replicate, using the RNAqueous-Micro Total RNA Isolation Kit (ThermoFisher Scientific). Total RNA was sent to The Yale Center for Genome Analysis for 75 nucleotide single-end sequencing in an Illumina HiSeq 2000.

Raw sequences were processed with Kallisto to quantify transcripts and Sleuth was used for differential abundance analysis (PIMENTEL *et al.* 2017), which generated an estimate for differential gene expression effect size termed "b" that is analogous to $\log_2$ fold change and an adjusted p-value termed "q". We analyzed six pairs of conditions from our experiment and a previously published pair of raw sequence data (GSE63075) (STEINBAUGH *et al.* 2015).

We considered genes differentially expressed if they had a q-value ≤ 0.05 and a b-value ≥ 1 or ≤ -1. All differentially expressed genes present in all conditions were clustered with Gene Cluster 3.0 using correlation (uncentered) average linkage and mapped with Java Treeview 1.1.6r4. Differentially expressed genes were tested for GO (Gene Ontology) analysis by DAVID 6.8 for gene functional classification using a high stringency (HUANG *et al.* 2009); classifications with a Benjamini adjusted p ≤ 0.05 are listed.

In vivo assays

Acute osmotic resistance assays were performed by counting the percentage of worms that responded to gentle touches with a worm pick after 10 min on an agar plate with 500 mM NaCl as described previously (WHEELER AND THOMAS 2006). Longevity and juglone resistance assays were performed as described previously (TANG AND CHOE 2015), except that instead

of using floxuridine (FUDR) for longevity studies on high NaCl, adults were manually transferred to fresh plates daily for the first few days to avoid mixing generations. Osmotic survival assays were performed by transferring worms from 51 to 450 mM NaCl agar plates and counting live and dead worms a day later.

Glycerol assays

Glycerol assays were conducted on populations of whole worms lysed by sonication using the PicoProbe™ Free Glycerol Fluorometric Assay Kit (Biovision). Values were normalized to total protein using the Pierce™ BCA Protein Assay Kit (ThermoFisher Scientific).

Statistical analysis

Statistical significance was determined using a student's T-test when two means were compared, a one-way analysis of variance with a Dunnet or Tukey's post-hoc test when three or more means were compared, a log-rank test when survival curves were compared, and a chi-square test for categorical reporter data. Overall p-values of < 0.05 were taken to indicate statistical significance. Bonferroni corrections to p-values were used when more than two survival curves were compared.

Reagent and data availability

Strains are available upon request. Raw numeric data are at https://figshare.com/s/7863ed7b6e2bed9e6510 and RNAseq raw data are at Gene Expression Omnibus (GSE107704).

RESULTS

RNAi screening identifies a specific cuticle structure required for regulation of detoxification, osmolyte, and antimicrobial responses

The cuticle is a complex extracellular matrix composed of over 100 distinct collagen proteins secreted from underlying epidermal cells. It forms a hydrostatic skeleton and acts as the primary barrier and first line of defense against many environmental insults (JOHNSTONE 2000; ALVAREZ *et al.* 2007; BURNS *et al.* 2010). The cuticle is composed of multiple layers, some with distinct structures discernable by light and/or electron microscopy. We used dsRNA feeding to disrupt diverse aspects of cuticle or epidermal integrity and test for induction of six stress response gene reporters: osmolyte accumulation (*gpdh-1*), antimicrobial (*nlp-29*), detoxification (*gst-4*), heat shock (*hsp-16.2*), and mitochondrial and endoplasmic reticulum unfolded protein (*hsp-6* and *hsp-4*, respectively). These stress responses are conserved and well-studied in *C. elegans* (JONES *et al.* 1989; SHEN *et al.* 2001; YONEDA *et al.* 2004; LAMITINA *et al.* 2006; PUJOL *et al.* 2008a).

Morphology phenotypes and reporter scores averaged over three trials are shown in Figure 1A, organized by morphology phenotype and strength of reporter induction. Results for the 19 of 40 dsRNA feeding clones that caused the most consistent morphology phenotypes are shown (grey shading), with variation between trials as is common with feeding clones (ZUGASTI *et al.* 2016). A test was considered positive if the reporter gene was induced in at least 5% of the worm population, in at least two of three trials (white outlined boxes). We report for the first time that silencing of four cuticle/epidermal integrity genes activates *gst-4p::GFP* as well as *gpdh-1p::DsRed2* and *nlp-29p::GFP*. We also observed acute osmotic stress resistance (OSR) when silencing the same genes (Figs. 1A, S1A, and Table S2), a phenotype associated with *gpdh-1* induction (WHEELER AND THOMAS 2006). The *hsp-16.2* and *hsp-6* reporters were not activated by any clones. Silencing of many other genes caused a diverse range of expected cuticle, morphology, and epidermal phenotypes (e.g., Dumpy, Blister, Roller, Long, Molting defect) but did not consistently activate *gst-4* or *gpdh-1* reporters. Together, these results suggest that detoxification and osmolyte responses are activated by silencing of a specific subset of *dpy* collagens and not by body shape or general epidermis disorganization. Consistent with previous studies (TONG *et al.* 2009; WARD *et al.* 2014; TAFFONI AND PUJOL 2015; ZUGASTI *et al.* 2016), the *nlp-29* reporter was activated by silencing of the same specific *dpy* genes, but was also activated by loss of genes that cause severe disruption of molting or epidermal integrity (*mlt-7*, *bli-4*, *klf-3*, and *mua-6*) and slightly by loss of *dpy-11*, which also activated *hsp-4*.

We also used a COPAS BIOSORT to quantify *nlp-29p::GFP* fluorescence with RNAi inactivation of 11 *dpy* genes (Figs. 1b and S1), nine of which overlap with Fig. 1A. These results confirmed strong activation of *nlp-29p::GFP* with *dpy-2*, *3*, *7*, and *10* and lack of strong activation with *dpy-11, 13*, *5*, *1*, and *20*; they also added *dpy-8* and *9* to the list of *dpy* clones activating *nlp-29p::GFP*. *nlp-29p::GFP* induction has also been confirmed in mutants of *dpy-9* and *10* (PUJOL *et al.* 2008b; ZUGASTI *et al.* 2014). Interestingly, mutants of *dpy-2, 3, 7, 8, 9*, and *10* were previously found to have no annular furrows but did have other cuticle structures including alae, which are lateral ridges in the cuticle perpendicular to furrows (COX *et al.* 1980; MCMAHON *et al.* 2003; THEIN *et al.* 2003); morphology and stress response results are summarized for *dpy* genes in Table S2.

To confirm the role of alae and furrows, we silenced *dpy-2, 3, 7,* and *10* and five other collagens with morphology phenotypes (*dpy-5, 11, 1, 13,* and *sqt-2*) in a strain of worm expressing COL-19::GFP, a collagen marker that labels the matrix of the circumferential transverse annuli and the tri-laminate lateral alae (THEIN *et al.* 2003). Similar to prior analysis of mutants, silencing of *dpy-2, 3, 7,* or *10* completely disrupted the wild-type parallel pattern of furrows without eliminating alae (Fig. 2). Conversely, silencing of *dpy-5* or *13* eliminated alae without disrupting furrows and silencing of *dpy-1* and *sqt-2* did not cause any obvious disruption to either alae or furrows.

Silencing *dpy-11* caused partial irregular branching of furrows and eliminated alae. Interestingly, it was only with *dpy-11* RNAi that we observed activation of the ER stress response reporter (*hsp-4*) together with weak activation of the antimicrobial reporter (*nlp-29*) (positive in 2/3 visual scoring trials and a non-significant 1.4 fold increase in BIOSORT quantification). Unlike most of the other Dpy genes tested, *dpy-11* does not encode a collagen but rather a nematode-specific protein with a thioredoxin domain (pfam00085). It is exclusively expressed in epidermal cells where is has been suggested to be localized to the endoplasmic reticulum or Golgi apparatus (KO AND CHOW 2002). It may be required for the maturation of cuticle collagens, but could also be involved in post-translational modification of other substrates, including signaling molecules linked to a distinct cellular stress pathway.

We next used quantitative PCR with two collagen mutants with disrupted furrows (*dpy-10(e128)* and *dpy-7(e88)*), one with intact furrows (*dpy-5(e61)*), and one reported to have more general alae and furrow disruption (*sqt-2(sc3)*) (THEIN *et al.* 2003). As shown in Figure 3, *gpdh-1*, *gst-4,* and *nlp-29* were induced in *dpy-10* and *dpy-7* worms, but not in *sqt-2* or *dpy-5* worms, similar to the RNAi results (Fig. 1). Another osmotic response gene (*hmit-1.1*) (KAGE-NAKADAI *et al.* 2011) was also induced only in *dpy-10* and *dpy-7* worms and detoxification response genes (*gst-10* and *gst-30*) were induced in *dpy-7* worms. Other stress responsive genes that we tested were not induced by any of the mutations.

Taken together, Figs. 1-3 suggest that specific loss of annular furrows, and not alteration of body shape, alae, or general epidermal integrity, initiates a signal that co-activates osmolyte accumulation, antimicrobial, and detoxification responses, but not all stress responses. The antimicrobial *nlp-29* reporter also responded to detachment of the cuticle (blister phenotype, *bli-4* and *mtl-7*), hemidesmosome disruption (*mua-6*), disruption of muscle/cuticle attachments (*klf*-3), and disruption of fatty acid metabolism (*acs-3* and *fasn-1*) (LEE *et al.* 2010; WARD *et al.* 2014); the *nlp-29* reporter also responded weakly to loss of thioredoxin domain encoding gene *dpy-11*. This is consistent with *nlp-29* activation upon a broader range of signals affecting epidermal integrity (PUJOL *et al.* 2008a; ZUGASTI *et al.* 2016).

Given that furrow mutants accumulate high levels of glycerol (LAMITINA *et al.* 2006; WHEELER AND THOMAS 2006), we speculated that detoxification, antimicrobial, and osmolyte accumulation stress responses could be induced in response to high internal osmolarity. As expected, *dpy-7(RNAi)* strongly induced glycerol accumulation in wild type worms (Fig. S1B). Deletions in both *gpdh* genes (*gpdh-1* and *2*) reduced glycerol accumulation by *dpy-7(RNAi)* almost completely, 87% (Fig. S1B). When measured by qPCR, *dpy-7(RNAi)* was able to significantly increase *gst-4*, *nlp-29*, and *hmit-1.1* mRNA levels in *gpdh* knockout worms, albeit by a reduced relative amount compared to wildtype in part because of elevated basal levels (Fig. S1C). Therefore, loss of furrows can activate stress responses without the majority of glycerol accumulation.

Role of skn-1 in gene expression during osmotic stress and in dpy-7 mutants

The transcription factor SKN-1 was previously reported to be important for detoxification responses under basal conditions and during oxidative stress (OLIVEIRA *et al.* 2009; PARK *et al.* 2009). We addressed the role of SKN-1 in *dpy-7(e88)* mutants and worms exposed to 300 mM NaCl for 3 h or 24 h with RNAseq. We also re-analyzed a previously published RNAseq dataset for *skn-1(RNAi)* under basal conditions (STEINBAUGH *et al.* 2015). Genes up regulated by *dpy-7(e88)* or osmotic stress were similar to those from previous studies of *dpy-10* mutants and osmotic stress (ROHLFING *et al.* 2010) and include osmolyte accumulation, pathogen response, and detoxification response (Table S3). As expected, *skn-1(RNAi)* reduced expression of many phase II detoxification genes (Table S3).

A heat map of genes differentially expressed in at least one of the seven comparisons and clustered by expression is shown in Figure 4 with a table of correlation coefficients below (Values are in Tables S4-5 and Gene Expression Omnibus, GSE107704) . The longer 24 h exposure to 300 mM NaCl had similar effects on expression as *dpy-7(e88)* (correlation coefficient of 0.77), and they both upregulated more genes than they downregulated. The shorter 3 h exposure to 300 mM NaCl had a smaller effect. The cluster of genes upregulated by high NaCl and *dpy-*

7(e88) is enriched for structural functions (cuticle collagen, nidogen, cadherin, and myosin-like) and detoxification (UGT (glycosyltransferase), cytochrome P450, GST (glutathione s-transferase), and ABC transporters, Fig. 4). The cluster of genes downregulated by 300 mM NaCl and *dpy-7(e88)* is enriched for cuticle collagen, F-box, and fatty acid metabolism. These data are consistent with gene expression responses to compensate for osmotically-induced mechanical stress and changes to metabolism.

Using our analysis pipeline applied to a previously published dataset, *skn-1(RNAi)* only downregulated 20 genes under basal conditions; *skn-1(RNAi)* only downregulated 1.2% of the genes upregulated by 3 h of 300 mM NaCl (Table S3). Alternatively, *skn-1(RNAi)* downregulated 4.1 and 12.1% of the genes upregulated by 24 h NaCl and *dpy-7(e88),* respectively. These data indicate that SKN-1 plays a larger role in gene regulation during chronic high NaCl and furrow loss than under basal conditions and short-term high NaCl exposure. The cluster of genes most strongly downregulated by *skn-1(RNAi)* in the heat map are enriched for detoxification and structural functions (top of Fig. 4), which is similar to enrichment within all genes upregulated by 24 h 300 mM NaCl and *dpy-7(e88)*. It is also clear in the heat map that many genes are induced independently of *skn-1*.

In Figure S2, we present Sleuth b and q-values for core genes of the six stress responses screened in Figure 1. Similar to the reporter data, *dpy-7* significantly activated genes of the osmotic, antimicrobial, and detoxification responses without activating other stress responses. Exposure to 300 mM NaCl had similar effects, particularly at 24 h. As expected, *skn-1(RNAi)* reduced induction of many phase II detoxification genes, particularly within the *gst* gene class. Surprisingly, expression of *gpdh-1* and *hmit-1.1* osmolyte accumulation genes were partially decreased by *skn-1(RNAi)* in *dpy-7(e88).* Upregulation of some antimicrobial genes was actually slightly enhanced by *skn-1(RNAi)* at 24 h NaCl and in *dpy-7(e88)*. Lastly, there were also many *ugt* and a few *gst* genes that were induced regardless of *skn-1(RNAi)* suggesting independent or compensatory mechanisms of regulation.

Annular furrow defects activate detoxification genes in the epidermis via SKN-1

Members of the *gst* gene class are well-established targets of SKN-1 and qPCR confirmed the requirement of *skn-1* for expression of *gst-4* and *gst-10* in *dpy-7(e88)* worms (Figs. 5A-B); these two direct targets are also under control of *skn-1* in wildtype worms (Figs. 5A-B). As shown in Figure 5C, a *gst-4p::GFP* reporter was activated in *dpy-10(e128)* worms in a *skn-1* dependent manner. We next used the *gst-4p::GFP* reporter and another SKN-1 target reporter, *gst-10p::GFP,* to identify the tissues in which detoxification genes were induced. In *dpy-10(e128)* and *dpy-7(RNAi*) worms, *gst-4p::GFP* and *gst-10p::GFP* fluorescence was predominantly visible in epidermal cells (Figs. 5D-G). This contrasts with the robust SKN-1 activation observed in the intestine during oxidative stress (AN AND BLACKWELL 2003; KELL *et al.* 2007; KAHN *et al.* 2008; CHOE *et al.* 2009). Exposure of *dpy-7(e88)* worms to acrylamide, a strong SKN-1 inducer, activated *gst-4p::GFP* strongly in the intestine (Fig. S3B) indicating that the intestinal detoxification response is still intact when furrows are disrupted.

High external osmolarity activates skn-1-dependent detoxification genes in the epidermis

Given the similar transcriptional profiles observed with high NaCl and *dpy-7(e88)* (Fig. 4), we next addressed the role of SKN-1 in gene regulation upon osmotic stress. As shown in Figures 6A-B, high concentrations of NaCl or sorbitol induced *gst-4p::GFP* by a *skn-1* dependent mechanism. Similar to *dpy-7* and *dpy-10* worms, the reporter was predominantly induced in the epidermis (Fig. 6C). qPCR confirmed induction of *gst-4* and another detoxification gene, *ugt-57*, *via skn-1* in worms exposed to 300 mM NaCl for three hours (Fig. 6D-E). Using a fluorescent plate reader, we observed induction of *gst-4p::GFP* by as little as 118 mM sorbitol (Fig. 6F), a level that has no obvious effects on worm health in our hands.

The *skn* gene generates three different transcripts (*skn-1a, b,* and *c*) sharing a common C-terminus but with alternative start sites, and our dsRNA clone targets all three. *gst-4* mRNA was fully induced by 300 mM NaCl and *dpy-7(RNAi)* in a recently engineered strain with a stop codon introduced into the first *skn-1a*-specific exon (Fig. S4A), consistent with either *skn-1b* or *c* functioning in these contexts. Although some pro-oxidants and genetic manipulations that induce the expression of *skn-1* dependent genes provoke nuclear accumulation of SKN-1b/c::GFP, there are also many conditions in which *skn-1* dependent genes are induced without visible nuclear accumulation (AN AND BLACKWELL 2003; KAHN *et al.* 2008; WU *et al.* 2016). These results are consistent with mechanisms that can increase gene expression *via* SKN-1 without increasing nuclear levels above what already exists under basal conditions. When accumulation does occur, it is most easily observed in the intestine and epidermis (WU *et al.* 2016). We used worms

expressing a SKN-1b/c::GFP fusion protein to determine if furrow disruption or high osmolarity cause nuclear accumulation of the transcription factor. We counted the number of worms with visible SKN-1b/c::GFP fluorescence when treated with *dpy-7(RNAi)*, *dpy-10(RNAi)*, 347 mM sorbitol, or 200 mM NaCl (Fig. 6G). We focused on the head epidermis, where *gst-4p::GFP* fluorescence is highest in furrow mutants (Fig. 5). As shown in Figure 6G, we observed accumulation of SKN-1b/c::GFP only with the positive control pro-oxidant juglone.

Osmolyte accumulation gene induction is partially dependent on skn-1

As mentioned above, our transcriptional analyses show that *skn-1(RNAi)* reduced the expression of some osmolyte accumulation genes after exposure to high concentrations of NaCl and in *dpy-7* worms (Fig. 4). This represents a novel function for SKN-1. To confirm these effects, we used qPCR and found that *gpdh-1* and *hmit-1.1* expression was partially, or fully, dependent on *skn-1* in worms exposed to 300 mM NaCl for 3 h and in *dpy-7* worms (Figs. 7A-D). On the other hand, *skn-1(RNAi)* had no effect on *gpdh-1* or *hmit-1.1* expression after 24 h on 300 mM NaCl corresponding to a time when glycerol levels approach a steady state (Figs. 7E-F) (LAMITINA *et al.* 2006). Under basal conditions in wildtype worms, *gpdh-1,* but not *hmit-1.1,* was partially dependent on *skn-1* (Fig. 7G-H).

We next measured whole-worm glycerol levels in *dpy-7* worms and worms exposed to 300 mM NaCl for 6 or 24 h, because previous studies reported high glycerol accumulation rates at 6 h and an elevated steady state glycerol level at 24 h (LAMITINA *et al.* 2004). As expected, glycerol was dramatically elevated by *dpy-7* mutation and high osmolarity (Figs. 7I-L). Loss of *skn-1* partially reduced glycerol levels in *dpy-7* worms (Fig. 7J), but not in worms exposed to high osmolarity (Figs. 7K-L). Taken together, these data indicate that in worms with disrupted annular furrows, *skn-1* is partially required for expression of osmotic-responsive genes and accumulation of glycerol. *skn-1* also plays a role in the initial induction of osmolyte accumulation genes by high osmolarity, but without a measurable effect on total glycerol levels.

Physiological assays with skn-1

We next tested if longevity or resistance to a pro-oxidant were altered in *dpy-10* or *dpy-7* worms as might be expected with constitutive activation of detoxification genes. As shown in Figure 8A, *dpy-7* and *dpy-10* worms had lifespans that were very similar to wildtype, and both were actually hyper-sensitive to the naturally occurring reactive small molecule juglone compared to wild-type worms (Fig. S4B). The cuticle is the nematode's primary barrier and its disruption is known to increase sensitivity to diverse small molecules (PARTRIDGE *et al.* 2008). The sensitivity of *dpy-7* and *dpy-10* worms is consistent with barrier disruption and this was also observed for *dpy-5* mutants (Fig. S4B) that do not exhibit an elevated level of *gst* gene expression (Fig. 3). Inactivation of *skn-1* further decreased survival (Fig. S4B), consistent with SKN-1 contributing generally to protection against oxidants.

We next conducted experiments to explore the influence of SKN-1 on survival in the presence of high NaCl. We first tested the effects of SKN-1 loss and activation using *skn-1* and *wdr-23(RNAi)*, respectively, on the ability of young adult worms to survive for a day after direct transfer from standard growth media containing 51 mM NaCl to media containing 450 mM NaCl. WDR-23 is a direct and robust repressor of SKN-1 (CHOE *et al.* 2009). Both *skn-1* and *wdr-23* RNAi increased survival under these conditions, although the effects were small (Fig. 8B). These effects suggest that SKN-1 manipulation has complex effects in survival of acute hyperosmotic exposure that might include compensatory responses.

We also tested the effect of *skn-1(RNAi)* on longevity under conditions of chronic high NaCl. It was recently demonstrated that high NaCl can increase longevity of *C. elegans*, but only in the presence of the DNA synthesis inhibitor 5-fluorodeoxyuridine, which is commonly used to prevent growth of progeny (ANDERSON *et al.* 2016). To circumvent this complication, we avoided progeny in these experiments by manually transferring adult worms to new plates. Lifespan was measured at 51 mM NaCl, 200 mM NaCl, and 500 mM NaCl. Worms had to first be grown on 200 mM NaCl before transferring to 500 mM at the early adult stage to allow larval development. Loss of *skn-1* decreased lifespan at 500 mM, but this was similar to the effect on standard 51 mM media (Fig. 8C) consistent with SKN-1 promoting lifespan in many contexts.

Distinct, but overlapping, transcription factors function downstream from furrow disruption

Transcriptional control of *gpdh-1* and *nlp-29* upon osmotic challenge in the *C. elegans* epidermis has been reported to be dependent on the ELT-3 GATA transcription factor (PUJOL *et al.* 2008b; ROHLFING *et al.* 2010). *nlp-29* also depends on the STAT transcription factor-like protein STA-2 during infection and wounding, but not high NaCl (DIERKING *et al.* 2011). ELT-3 has been postulated to cooperate with a number of transcription factors, including SKN-1 and

STA-2 to permit stress responses in the epidermis (BLOCK and SHAPIRA, 2015). We tested the effects of RNAi for *elt-3*, *sta-2,* and *skn-1* on *gpdh-1, gst-4*, and *nlp-29* reporter induction in *dpy-7* furrow mutants (Fig 9). Note that while *gst-4p::GFP* and *nlp-29p::GFP* are primarily epidermal in this context, *gpdh-1p::DsRed2* is active in the intestine and epidermis and fluorescence levels are from whole-worms. RNAi of *skn-1* decreased *gpdh-1p::DsRed2* and *gst-4p::GFP* confirming a shared requirement; *skn-1(RNAi)* actually slightly increased *nlp-29p::GFP* (Fig. 9), which was also observed for *nlp-29* mRNA in RNAseq analysis (Fig. S2). RNAi of *elt-3* decreased *gst-4p::GFP* and *nlp-29p::GFP* significantly, but did not have a significant effect on total *gpdh-1p::DsRed2* fluorescence (Fig. 9). RNAi of *sta-2* decreased *gpdh-1p::DsRed2* and *nlp-29p::GFP*, but not *gst-4p::GFP*. Using mutants in *dpy-3, dpy-7,* and *dpy-10* worms, we confirmed the requirements of *sta-2* and *elt-3* for *nlp-19p::GFP* (Fig. S4C). Collectively, the results in Figures 9 and S4 suggest that disruption of furrows in the cuticle activates osmotic, detoxification, and antimicrobial transcriptional responses *via* distinct, but overlapping, downstream transcription factors (Fig. 10).

DISCUSSION

Co-regulation of three stress responses via cuticle furrows

The cortical layer of the adult *C. elegans* cuticle contains lateral ridges of collagen called alae and circumferential bands called annular furrows. Annular furrows were previously implicated in regulation of *gpdh-1* from a genome-wide RNAi screen (LAMITINA *et al.* 2006; WHEELER AND THOMAS 2006; CHOE 2013). Two collagen mutants with furrow defects were also previously shown to have high *nlp-29* expression (PUJOL *et al.* 2008b), but it was unknown if other cuticle/epidermal characteristics and stress responses were involved.

Mutation or silencing of six collagen genes (*dpy-2, 3, 7, 8, 9,* and *10*) severely disrupts furrows without eliminating alae (COX *et al.* 1980; MCMAHON *et al.* 2003; THEIN *et al.* 2003) (Fig. 2 and Table S2). We demonstrate that genetic manipulations that specifically disrupt furrows co-activate osmolyte accumulation, *nlp-29,* and *skn-1* dependent detoxification genes but do not activate responses to heat-shock, mitochondrial unfolded proteins, or endoplasmic reticulum unfolded proteins (Figs. 1-3, and S2). Therefore, our results are consistent with a requirement for annular furrows in regulating osmolyte accumulation, antimicrobial, and *skn-1* dependent detoxification genes, but not all stress responses.

The cuticle and underlying epidermis form the primary barrier between tissues and the environment and are therefore well-positioned to detect and respond to stress. Recent atomic force microscopy analyses revealed high biomechanical stiffness at furrows relative to annuli (ESSMANN *et al.* 2017). Nematode body morphology is supported by turgor pressure against the body wall. Hypertonicity-induced water loss depletes turgor pressure in *C. elegans* and the epidermis and cuticle become physically distorted (LAMITINA *et al.* 2004; CHOE 2013). Given that furrows are circumferential bands of collagen in the cuticle, we speculate that mechanical strain on these structures likely changes with turgor pressure against the body wall. Physical distortion of furrows or changes in associated extracellular ligand availability could signal *via* membrane receptors such as integrins, G-protein coupled receptors, phospholipases, enzyme-linked receptors, or ion channels (CLAUSE AND BARKER 2013; ROSS *et al.* 2013; SCHILLER AND FASSLER 2013; GASPARSKI AND BENINGO 2015). Interestingly, loss of a protein secreted by the epidermis named OSM-11 co-activates osmolyte synthesis, detoxification, and antimicrobial genes (WHEELER AND THOMAS 2006; PUJOL *et al.* 2008b; DRESEN *et al.* 2015) without causing any obvious cuticle defects. OSM-11 is thought to act as a ligand for Notch receptors to regulate vulva development and behavior (KOMATSU *et al.* 2008; SINGH *et al.* 2011). It remains to be seen if Notch signaling plays a role in transmitting signals from the cuticle. It will also be interesting to examine whether hypoosmotic-induced increases in turgor pressure are also able to initiate signals to stress responses.

A G-protein coupled receptor named DCAR-1 is partially required for induction of *nlp-29* in the furrow mutants *dpy-9* and *dpy-10*, but was not required for transcriptional activation of *nlp-29* upon osmotic stress (ZUGASTI *et al.* 2014). These results suggest that different receptors might be activated downstream from a common furrow-associated sensor.

Distinct transcription factor requirements downstream of furrow disruption

In yeast, at least four transcription factors downstream from an osmosensor-associated protein named HOG1 (hyperosmolarity glycerol response 1) activate downstream genes (HOHMANN *et al.* 2007). In mammalian cells, the hypertonicity enhancer binding protein (TonEBP), also known as NFAT5, regulates a battery of genes responsible for organic osmolyte accumulation and cytoprotection (LEE *et al.* 2011). *C. elegans* lacks a close homolog of TonEBP and instead GATA transcription factor *elt-3* is at least partially required for *gpdh-1* and *nlp-29* induction by high NaCl

in the epidermis (PUJOL *et al.* 2008b; ROHLFING *et al.* 2010).

Our results are consistent with distinct, but partially overlapping, transcriptional pathways functioning downstream from furrow loss to activate distinct stress responses (Fig. 10). Interestingly, elt-3 in addition to skn-1 is required for the detoxification response to furrow loss (Fig. 9). Similarly, elt-3 and skn-1 were recently shown to co-regulate detoxification genes in a stress-sensitive mutant (HU *et al.* 2017). Conversely, *sta-2* is completely required and *elt-3* partially required for the antimicrobial response in the epidermis (Fig. 9 and S4B). We found evidence for a novel role for *skn-1* in induction of *gpdh-1* (Figs. 7 and 9). SKN-1 binding elements (SBE) were previously defined (BLACKWELL *et al.* 1994; RUPERT *et al.* 1998), but we found none within 3 kb upstream of *gpdh-1* nor *hmit-1.1* start codons suggesting indirect regulation.

SKN-1 dependent gene induction

Regulation of intracellular SKN-1/Nrf signaling in response to reactive small molecules is well-studied in mammalian cells and C. elegans (Taguchi et al. 2011; Niture et al. 2013; Blackwell et al. 2015; Wu et al. 2016; Wu et al. 2017). Conversely, very little is known about regulation of SKN-1/Nrf pathways via the extracellular matrix. A lack of obvious increases in nuclear accumulation (Fig. 6G) is consistent with regulation by post-translational modification or by changes in interaction with DNA or co-factors.

Antioxidant/detoxification pathways protect tissues from inflammation and fibrosis, making coordination of Nrf2 signaling and the extracellular matrix important to disease pathogenesis (WU *et al.* 2015; AHMED *et al.* 2017; XU *et al.* 2017). In cultured mammalian vascular cells, Nrf2-dependent responses have been shown to be activated by mechanical shear stress that models turbulent blood flow, with intracellular reactive oxygen species (ROS) being implicated as a downstream signal (JONES *et al.* 2007; WARABI *et al.* 2007; HSIEH *et al.* 2014). It is not known how the extracellular mechanical stimulus is detected and transduced into the cell where ROS are generated. It was recently shown that a *skn-1*-dependent detoxification response could be activated by an increase in ROS at the ER *via* sulfenylation of the kinase IRE-1 (HOURIHAN *et al.* 2016). It remains to be seen if ROS are increased in furrow mutants through the action of an endogenous enzyme. Signaling mechanisms that act downstream of annular furrow disruption to activate SKN-1 mediated transcriptional responses will define a novel mode of signaling for this conserved family of stress and longevity factors.

ACKNOWLEDGMENTS

We thank Jonathan Ewbank for comments on the manuscript and Gary Ruvkun for sharing the *skn-1a(mg570)* allele. *C. elegans* strains were provided by the *Caenorhabditis* Genetics Center (University of Minnesota, Minneapolis, MN) supported by the National Institutes of Health Office of Research Infrastructure Programs (P40 OD010440). This study was supported by NSF grants IOS-1120130 and IOS-1452948 to KPC, an NSERC postdoctoral fellowship to CWW, and by institutional grants from AMU, INSERM and CNRS, the ANR-11-LABX-0054 (Investissements d'Avenir–Labex INFORM) and ANR-11-IDEX-0001-02 (Investissements d'Avenir–A*MIDEX) to NP. All authors participated in conducting experiments and analyzing and interpreting data. KPC and NP wrote the manuscript. All authors approved the final version of the manuscript.

REFERENCES

Ahmed, S. M., L. Luo, A. Namani, X. J. Wang and X. Tang, 2017 Nrf2 signaling pathway: Pivotal roles in inflammation. Biochim Biophys Acta 1863**:** 585-597.

Alvarez, L. I., M. L. Mottier and C. E. Lanusse, 2007 Drug transfer into target helminth parasites. Trends Parasitol 23**:** 97-104.

An, J. H., and T. K. Blackwell, 2003 SKN-1 links *C. elegans* mesendodermal specification to a conserved oxidative stress response. Genes Dev. 17**:** 1882-1893.

Anderson, E. N., M. E. Corkins, J. C. Li, K. Singh, S. Parsons *et al.*, 2016 *C. elegans* lifespan extension by osmotic stress requires FUdR, base excision repair, FOXO, and sirtuins. Mech Ageing Dev 154**:** 30-42.

Blackwell, T. K., B. Bowerman, J. R. Priess and H. Weintraub, 1994 Formation of a monomeric DNA binding domain by SKN-1 bZIP and homeodomain elements. Science 266**:** 621-628.

Blackwell, T. K., M. J. Steinbaugh, J. M. Hourihan, C. Y. Ewald and M. Isik, 2015 SKN-1/Nrf, stress responses, and aging in *Caenorhabditis elegans*. Free Radic Biol Med 88**:** 290-301.

Brenner, S., 1974 The genetics of *Caenorhabditis elegans*. Genetics 77**:** 71-94.

Bryan, H. K., A. Olayanju, C. E. Goldring and B. K. Park, 2013 The Nrf2 cell defence pathway: Keap1-dependent and -independent mechanisms of regulation. Biochem Pharmacol 85**:** 705-717.

Burns, A. R., I. M. Wallace, J. Wildenhain, M. Tyers, G. Giaever *et al.*, 2010 A predictive model for drug bioaccumulation and bioactivity in *Caenorhabditis elegans*. Nat Chem Biol 6**:** 549-557.

Chisholm, A. D., and S. Xu, 2012 The *Caenorhabditis elegans* epidermis as a model skin. II: differentiation and physiological roles. Wiley Interdiscip Rev Dev Biol 1**:** 879-902.

Choe, K. P., 2013 Physiological and molecular mechanisms of salt and water homeostasis in the nematode *Caenorhabditis elegans*. Am J Physiol Regul Integr Comp Physiol 305**:** R175-186.

Choe, K. P., C. K. Leung and M. M. Miyamoto, 2012 Unique structure and regulation of the nematode detoxification gene regulator, SKN-1: implications to understanding and controlling drug resistance. Drug Metab Rev 44**:** 209-223.

Choe, K. P., A. J. Przybysz and K. Strange, 2009 The WD40 repeat protein WDR-23 functions with the CUL4/DDB1 ubiquitin ligase to regulate nuclear abundance and activity of SKN-1 in *Caenorhabditis elegans*. Mol Cell Biol 29**:** 2704-2715.

Clause, K. C., and T. H. Barker, 2013 Extracellular matrix signaling in morphogenesis and repair. Curr Opin Biotechnol 24**:** 830-833.

Cox, G. N., J. S. Laufer, M. Kusch and R. S. Edgar, 1980 Genetic and phenotypic characterization of roller mutants of *Caenorhabditis elegans*. Genetics 95**:** 317-339.

Dierking, K., J. Polanowska, S. Omi, I. Engelmann, M. Gut *et al.*, 2011 Unusual regulation of a STAT protein by an SLC6 family transporter in C. elegans epidermal innate immunity. Cell Host Microbe 9**:** 425-435.

Dresen, A., S. Finkbeiner, M. Dottermusch, J. S. Beume, Y. Li *et al.*, 2015 *Caenorhabditis elegans* OSM-11 signaling regulates SKN-1/Nrf during embryonic development and adult longevity and stress response. Dev Biol 400**:** 118-131.

Essmann, C. L., M. Elmi, M. Shaw, G. M. Anand, V. M. Pawar *et al.*, 2017 In-vivo high resolution AFM topographic imaging of *Caenorhabditis elegans* reveals previously unreported surface structures of cuticle mutants. Nanomedicine 13**:** 183-189.

Gaggar, A., and N. Weathington, 2016 Bioactive extracellular matrix fragments in lung health and disease. J Clin Invest 126**:** 3176-3184.

Gasparski, A. N., and K. A. Beningo, 2015 Mechanoreception at the cell membrane: More than the integrins. Arch Biochem Biophys 586**:** 20-26.

Hay, E. D., 1981 Extracellular matrix. J Cell Biol 91**:** 205s-223s.

Hobert, O., 2002 PCR fusion-based approach to create reporter gene constructs for expression analysis in transgenic *C. elegans*. Biotechniques 32**:** 728-730.

Hohmann, S., M. Krantz and B. Nordlander, 2007 Yeast osmoregulation. Methods Enzymol 428**:** 29-45.

Hourihan, J. M., L. E. Moronetti Mazzeo, L. P. Fernandez-Cardenas and T. K. Blackwell, 2016 Cysteine sulfenylation directs IRE-1 to activate the SKN-1/Nrf2 antioxidant response. Mol Cell 63**:** 553-566.

Hsieh, H. J., C. A. Liu, B. Huang, A. H. Tseng and D. L. Wang, 2014 Shear-induced endothelial mechanotransduction: the interplay between reactive oxygen species (ROS) and nitric oxide (NO) and the pathophysiological implications. J Biomed Sci 21**:** 3.

Hu, Q., D. R. D'Amora, L. T. MacNeil, A. J. M. Walhout and T. J. Kubiseski, 2017 The oxidative stress response in *Caenorhabditis elegans* requires the GATA transcription factor ELT-3 and SKN-1/Nrf2. Genetics**:** 116.198788.

Hu, R., C. Xu, G. Shen, M. R. Jain, T. O. Khor *et al.*, 2006 Identification of Nrf2-regulated genes induced by chemopreventive isothiocyanate PEITC by oligonucleotide microarray. Life Sciences 79**:** 1944-1955.

Huang, D. W., B. T. Sherman and R. A. Lempicki, 2009 Systematic and integrative analysis of large gene lists using DAVID bioinformatics resources. Nat Protoc 4**:** 44-57.

Johnstone, I. L., 2000 Cuticle collagen genes: expression in *Caenorhabditis elegans*. Trends in Genetics 16**:** 21-27.

Jones, C. I., 3rd, H. Zhu, S. F. Martin, Z. Han, Y. Li *et al.*, 2007 Regulation of antioxidants and phase 2 enzymes by shear-induced reactive oxygen species in endothelial cells. Ann Biomed Eng 35**:** 683-693.

Jones, D., D. K. Dixon, R. W. Graham and E. P. Candido, 1989 Differential regulation of closely related members of the hsp16 gene family in *Caenorhabditis elegans*. DNA 8**:** 481-490.

Kage-Nakadai, E., T. Uehara and S. Mitani, 2011 H^+/myo-inositol transporter genes, *hmit-1.1* and *hmit-1.2*, have roles in the osmoprotective response in *Caenorhabditis elegans*. Biochem Biophys Res Commun 410**:** 471-477.

Kahn, N. W., S. L. Rea, S. Moyle, A. Kell and T. E. Johnson, 2008 Proteasomal dysfunction activates the transcription factor SKN-1 and produces a selective oxidative-stress response in *Caenorhabditis elegans*. Biochem J 409**:** 205-213.

Kamath, R. S., A. G. Fraser, Y. Dong, G. Poulin, R. Durbin *et al.*, 2003 Systematic functional analysis of the *Caenorhabditis elegans* genome using RNAi. Nature 421**:** 231-237.

Kamath, R. S., M. Martinez-Campos, P. Zipperlen, A. G. Fraser and J. Ahringer, 2001 Effectiveness of specific RNA-mediated interference through ingested double-stranded RNA in *Caenorhabditis elegans*. Genome Biol 2**:** research0002.0001-0002.0010.

Kell, A., N. Ventura, N. Kahn and T. E. Johnson, 2007 Activation of SKN-1 by novel kinases in *Caenorhabditis elegans*. Free Radical Biology and Medicine 43**:** 1560-1566.

Ko, F. C., and K. L. Chow, 2002 A novel thioredoxin-like protein encoded by the *C. elegans dpy-11* gene is required for body and sensory organ morphogenesis. Development 129**:** 1185-1194.

Komatsu, H., M. Y. Chao, J. Larkins-Ford, M. E. Corkins, G. A. Somers *et al.*, 2008 OSM-11 facilitates LIN-12 Notch signaling during *Caenorhabditis elegans* vulval development. PLoS Biol 6**:** e196.

Lamitina, S. T., R. Morrison, G. W. Moeckel and K. Strange, 2004 Adaptation of the nematode *Caenorhabditis elegans* to extreme osmotic stress. Am J Physiol Cell Physiol 286**:** C785-791.

Lamitina, T., C. G. Huang and K. Strange, 2006 Genome-wide RNAi screening identifies protein damage as a regulator of osmoprotective gene expression. PNAS 103**:** 12173-12178.

Lee, K. Z., M. Kniazeva, M. Han, N. Pujol and J. J. Ewbank, 2010 The fatty acid synthase fasn-1 acts upstream of WNK and Ste20/GCK-VI kinases to modulate antimicrobial peptide expression in *C. elegans* epidermis. Virulence 1**:** 113-122.

Lee, S. D., S. Y. Choi, S. W. Lim, S. T. Lamitina, S. N. Ho *et al.*, 2011 TonEBP stimulates multiple cellular pathways for adaptation to hypertonic stress: organic osmolyte-dependent and -independent pathways. Am J Physiol Renal Physiol 300**:** F707-715.

Leung, C. K., A. Deonarine, K. Strange and K. P. Choe, 2011 High-throughput screening and biosensing with fluorescent *C. elegans* strains. J Vis Exp**:** e2745.

McMahon, L., J. M. Muriel, B. Roberts, M. Quinn and I. L. Johnstone, 2003 Two sets of interacting collagens form functionally distinct substructures within a *Caenorhabditis elegans* extracellular matrix. Mol. Biol. Cell 14**:** 1366-1378.

Niture, S. K., R. Khatri and A. K. Jaiswal, 2013 Regulation of Nrf2 - An update. Free Radic Biol Med 66**:** 36-44.

Oliveira, R. P., J. P. Abate, K. Dilks, J. Landis, J. Ashraf *et al.*, 2009 Condition-adapted stress and longevity gene regulation by *Caenorhabditis elegans* SKN-1/Nrf. Aging Cell 8**:** 524-541.

Page, A. P., and I. L. Johnstone, 2007 The cuticle, pp. in *WormBook*, edited by *C. e.* r. c. The. C. elegans Research Community The.

Park, S.-K., P. M. Tedesco and T. E. Johnson, 2009 Oxidative stress and longevity in *Caenorhabditis elegans* as mediated by SKN-1. Aging Cell 8**:** 258-269.

Partridge, F. A., A. W. Tearle, M. J. Gravato-Nobre, W. R. Schafer and J. Hodgkin, 2008 The *C. elegans* glycosyltransferase BUS-8 has two distinct and essential roles in epidermal morphogenesis. Dev Biol 317**:** 549-559.

Pimentel, H., N. L. Bray, S. Puente, P. Melsted and L. Pachter, 2017 Differential analysis of RNA-seq incorporating quantification uncertainty. Nat Methods 14**:** 687-690.

Pujol, N., S. Cypowyj, K. Ziegler, A. Millet, A. Astrain *et al.*, 2008a Distinct innate immune responses to infection and wounding in the *C. elegans* epidermis. Curr Biol 18**:** 481-489.

Pujol, N., O. Zugasti, D. Wong, C. Couillault, C. L. Kurz *et al.*, 2008b Anti-fungal innate immunity in *C. elegans* is enhanced by evolutionary diversification of antimicrobial peptides. PLoS Pathog 4**:** e1000105.

Rohlfing, A. K., Y. Miteva, S. Hannenhalli and T. Lamitina, 2010 Genetic and physiological activation of osmosensitive gene expression mimics transcriptional signatures of pathogen infection in *C. elegans*. PLoS One 5**:** e9010.

Rohlfing, A. K., Y. Miteva, L. Moronetti, L. He and T. Lamitina, 2011 The *Caenorhabditis elegans* mucin-like protein OSM-8 negatively regulates osmosensitive physiology via the transmembrane protein PTR-23. PLoS Genet 7**:** e1001267.

Ross, T. D., B. G. Coon, S. Yun, N. Baeyens, K. Tanaka *et al.*, 2013 Integrins in mechanotransduction. Curr Opin Cell Biol 25**:** 613-618.

Rozario, T., and D. W. DeSimone, 2010 The extracellular matrix in development and morphogenesis: a dynamic view. Dev Biol 341**:** 126-140.

Rual, J. F., J. Ceron, J. Koreth, T. Hao, A. S. Nicot *et al.*, 2004 Toward improving *Caenorhabditis elegans* phenome mapping with an ORFeome-based RNAi library. Genome Res. 14**:** 2162-2168.

Rupert, P. B., G. W. Daughdrill, B. Bowerman and B. W. Matthews, 1998 A new DNA-binding motif in the Skn-1 binding domain-DNA complex. Nat Struct Biol 5**:** 484-491.

Samarakoon, R., J. M. Overstreet and P. J. Higgins, 2013 TGF-beta signaling in tissue fibrosis: redox controls, target genes and therapeutic opportunities. Cell Signal 25**:** 264-268.

Schiller, H. B., and R. Fassler, 2013 Mechanosensitivity and compositional dynamics of cell-matrix adhesions. EMBO Rep 14**:** 509-519.

Shen, X., R. E. Ellis, K. Lee, C. Y. Liu, K. Yang *et al.*, 2001 Complementary signaling pathways regulate the unfolded protein response and are required for *C. elegans* development. Cell 107**:** 893-903.

Singh, K., M. Y. Chao, G. A. Somers, H. Komatsu, M. E. Corkins *et al.*, 2011 *C. elegans* Notch signaling regulates adult chemosensory response and larval molting quiescence. Curr Biol 21**:** 825-834.

Steinbaugh, M. J., S. D. Narasimhan, S. Robida-Stubbs, L. E. Moronetti Mazzeo, J. M. Dreyfuss *et al.*, 2015 Lipid-mediated regulation of SKN-1/Nrf in response to germ cell absence. Elife 4**:** 10.7554/eLife.07836.

Sykiotis, G., and D. Bohmann, 2010 Stress-activated cap'n'collar transcription factors in aging and human disease. Sci Signal 3**:** re3.

Taffoni, C., and N. Pujol, 2015 Mechanisms of innate immunity in *C. elegans* epidermis. Tissue Barriers 3**:** e1078432.

Taguchi, K., H. Motohashi and M. Yamamoto, 2011 Molecular mechanisms of the Keap1-Nrf2 pathway in stress response and cancer evolution. Genes Cells 16**:** 123-140.

Tang, L., and K. P. Choe, 2015 Characterization of *skn-1/wdr-23* phenotypes in *Caenorhabditis elegans*; pleitrophy, aging, glutathione, and interactions with other longevity pathways. Mech Ageing Dev 149**:** 88-98.

Thakur, N., N. Pujol, L. Tichit and J. J. Ewbank, 2014 Clone mapper: an online suite of tools for RNAi experiments in *Caenorhabditis elegans*. G3 (Bethesda) 4**:** 2137-2145.

Thein, M. C., G. McCormack, A. D. Winter, I. L. Johnstone, C. B. Shoemaker *et al.*, 2003 *Caenorhabditis elegans* exoskeleton collagen COL-19: an adult-specific marker for collagen modification and assembly, and the analysis of organismal morphology. Dev Dyn 226**:** 523-539.

Tong, A., G. Lynn, V. Ngo, D. Wong, S. L. Moseley *et al.*, 2009 Negative regulation of *Caenorhabditis elegans* epidermal damage responses by death-associated protein kinase. Proc Natl Acad Sci U S A 106**:** 1457-1461.

Warabi, E., W. Takabe, T. Minami, K. Inoue, K. Itoh *et al.*, 2007 Shear stress stabilizes NF-E2-related factor 2 and induces antioxidant genes in endothelial cells: role of reactive oxygen/nitrogen species. Free Radic Biol Med 42**:** 260-269.

Ward, J. D., B. Mullaney, B. J. Schiller, D. He le, S. E. Petnic *et al.*, 2014 Defects in the *C. elegans* acyl-CoA synthase, acs-3, and nuclear hormone receptor, nhr-25, cause sensitivity to distinct, but overlapping stresses. PLoS One 9**:** e92552.

Wheeler, J. M., and J. H. Thomas, 2006 Identification of a novel gene family involved in osmotic stress response in *Caenorhabditis elegans*. Genetics 174**:** 1327-1336.

Winograd-Katz, S. E., R. Fassler, B. Geiger and K. R. Legate, 2014 The integrin adhesome: from genes and proteins to human disease. Nat Rev Mol Cell Biol 15**:** 273-288.

Wu, C.-W., A. Deonarine, A. Przybysz, K. Strange and K. P. Choe, 2016 The Skp1 homologs SKR-1/2 are required for the Caenorhabditis elegans SKN-1 antioxidant/detoxification response independently of p38 MAPK. PLoS Genetics 12**:** e1006361.

Wu, C. W., Y. Wang and K. P. Choe, 2017 F-box protein XREP-4 Is a new regulator of the oxidative stress response in *Caenorhabditis elegans*. Genetics 206**:** 859-871.

Wu, H., L. Kong, Y. Cheng, Z. Zhang, Y. Wang *et al.*, 2015 Metallothionein plays a prominent role in the prevention of diabetic nephropathy by sulforaphane via up-regulation of Nrf2. Free Radic Biol Med 89**:** 431-442.

Xu, Y., W. Tai, X. Qu, W. Wu, Z. Li *et al.*, 2017 Rapamycin protects against paraquat-induced pulmonary fibrosis: Activation of Nrf2 signaling pathway. Biochem Biophys Res Commun 490**:** 535-540.

Yoneda, T., C. Benedetti, F. Urano, S. G. Clark, H. P. Harding *et al.*, 2004 Compartment-specific perturbation of protein handling activates genes encoding mitochondrial chaperones. J Cell Sci 117**:** 4055-4066.

Zugasti, O., N. Bose, B. Squiban, J. Belougne, C. L. Kurz *et al.*, 2014 Activation of a G protein-coupled receptor by its endogenous ligand triggers the innate immune response of *Caenorhabditis elegans*. Nat Immunol 15**:** 833-838.

Zugasti, O., N. Thakur, J. Belougne, B. Squiban, C. L. Kurz *et al.*, 2016 A quantitative genome-wide RNAi screen in *C. elegans* for antifungal innate immunity genes. BMC Biol 14**:** 35.

FIGURE LEGENDS

Figure 1. Genetic disruption of specific *dpy* genes activates detoxification, antimicrobial, and osmotic stress responses. (A) dsRNA expressing clones for genes required for diverse aspects of cuticle and epidermal integrity were scored for cuticle and morphology phenotypes and induction of stress response reporters. Stress response reporters were scored for penetrance and averaged together across three trials. Cuticle and morphology phenotype penetrance and expressivity (Dpy only) were scored and averaged together across three trials for each reporter line. Positive controls for reporters were 200 mM NaCl for *gpdh-1* and *nlp-29*, *wdr-23(RNAi)* for *gst-4*, 34ºC for 1 h for *hsp-16.2*, 0.5 mM paraquat for *hsp-6*, and 10 µg/mL tunicamycin for *hsp-4*. ND, not determined. Reporter results outlined with a thick white boarder were positive in at least two of three trials. Percent acute osmotic stress resistance (OSR, from trial run in Fig. 1B) and the presence (Yes) or absence (No) of intact furrows and alae (from Fig. 2) are also summarized. (B) The ratio of *nlp-29p::GFP* to time of flight (TOF) was measured in a BIOSORT and normalized to the negative control *sta-1(RNAi)*. *n* = 99-228 worms. Boxes are 25% percentiles above and below the median and whiskers are minimum and maximum.

Figure 2. The cuticle furrow is disrupted by *dpy* dsRNA clones that activate stress responses. A model of cortical cuticle structures and fluorescent micrographs of COL-19::GFP in worms treated with RNAi. Images are representative of 10 worms. Scale bar is 10 □M.

Figure 3. qPCR verification of stress response gene expression. mRNA levels for stress inducible genes in four collagen mutants. *n* = 3-9 replicates of worms combined from 1 or 2 trials. **P < 0.05*, ***P < 0.01*, and ****P < 0.001* relative to N2, which was normalized to a mean of 1.0.

Figure 4. Heat map of differentially expressed genes clustered by relative expression change. All 1594 genes that were differentially expressed in at least one of the seven comparisons and present in all conditions tested are included. Average sleuth analysis estimates of expression effect size for each comparison ('b') are provided on a $\log_2$ scale from decreased (blue) to increased (yellow). Correlation coefficients are provided below the heat map. GSE63075 data from N2 with and without *skn-1(RNAi)* (STEINBAUGH *et al.* 2015) are included. Gene functional category enrichments are from DAVID 6.8. *n* = 3 replicates of worms per treatment.

Figure 5. Disruption of cuticle annular furrows activates *skn-1*-dependent detoxification genes in the epidermis. (A-B) mRNA levels for *gst-4* and *gst-10* with and without *skn-1(RNAi)* in *dpy-7(e88)* worms (left graphs); results for *skn-1(RNAi)* in N2 worms are included for reference (right graphs). ***P < 0.001* and ****P < 0.001* relative to *dpy-7* or control. (C) *gst-4p::GFP* fluorescence images in N2, *dpy-10(e128)*, and *dpy-10(e128);skn-1(RNAi)* worms. (D-E) *gst-4p::GFP* in *dpy-10(e128)* worms; images taken at the focal plane of the intestine are paired with a differential interference contrast micrograph. (F-G) *gst-10p::GFP* in *dpy-7(RNAi)* worms; images taken at the focal plane of the intestine are paired with a differential interference contrast micrograph. (D-G) Broken lines mark the boundaries for the intestine (left) or epidermis (right).

Figure 6. High osmolarity activates *skn-1*-dependent detoxification genes in the epidermis. *gst-4p::GFP* is induced in worms exposed to 400 mM NaCl (A) or 652 mM sorbitol (B) and suppressed by *skn-1(RNAi)* (****P < 0.001*); low (dim signal limited to a few spots), medium (dim signal throughout the epidermis or bright signal only in head or tails regions), and high (bright signal throughout the epidermis); (C) Paired fluorescent and differential interference contrast images of the intestine (left) and epidermis (right) of a worm exposed to 400 mM NaCl. (D-E) Relative *gst-4* and *ugt-57* mRNA levels in worms exposed to 300 mM NaCl for three hours with and without *skn-1(RNAi)*. (**P < 0.05, **P < 0.01,* and ****P < 0.001* versus 300 mM*, n* = 4-5 populations of worms). (F) *gst-4p::GFP* fluorescence levels in worms exposed to a range of sorbitol concentrations overnight. *n* = 16 microplate wells. (G) Number of worms with and without nuclear SKN-1::GFP in the head region observed with confocal microscopy. No SKN-1::GFP was observed in the intestine under any conditions.

Figure 7. Induction of osmolyte synthesis genes partially requires *skn-1*. (A-B) Relative *gpdh-1* and *hmit-1.1* mRNA levels in *dpy-7(e88)* worms with and without *skn-1(RNAi)*. (C-F) Relative *gpdh-1* and *hmit-1.1* mRNA levels in worms exposed to 300 mM NaCl for 3 h (C-D) or 24 h (E-F) with and without *skn-1(RNAi)*. (G-H) Relative *gpdh-1* and *hmit-1.1* mRNA levels in N2 with and without *skn-1(RNAi)*. (**P < 0.05* versus *dpy-7* (A-B)*,* 300 mM NaCl (C-D), or control (G-H); *n* = 3-4 replicates of worms). (I-J) Whole worm glycerol levels in N2 and *dpy-7(e88)* worms with and without *skn-1(RNAi)*. *n* = 7-9 replicates from two trials. **P < 0.05*. (K-L)

Whole worm glycerol levels in worms exposed to 300 mM NaCl for 6 (K) or 24 h (L) with and without *skn-1(RNAi)*. *n* = 3-5 replicates of worms from one trial.

Figure 8. Physiological assays for *skn-1*. (A) Survival curves for longevity. *P > 0.7095* for *dpy-7* and *dpy-10* relative to N2. *n > 150* worms from two trials combined. (B) Survival, after 24 h, of *skn-1* and *wdr-23(RNAi)* worms transferred directly from 51 to 450 mM NaCl agar. ***P < 0.05* and ***P < 0.01* relative to *control(RNAi)*, *n* = 4 trials of 30-581 worms. (C) Survival of chronic exposure to high NaCl. All worms were treated from L1 larval stage except for 500 mM NaCl; these worms were grown on 200 mM NaCl until young adults and then transferred to 500 mM NaCl. *n* = 234-342 worms from three trials. *P < 0.001* for *skn-1(RNAi)* at 51 and 500 mM NaCl and *P = 0.0254* for *skn-1(RNAi)* at 200 mM NaCl.

Figure 9. Transcription factor requirements. (A and B) Worms grown to the gravid adult stage were mounted on slides and imaged. Image J was used to measure pixel intensity of individual worms on the GFP (A) or RFP (B) filter sets and values were normalized to the mean of *control(RNAi)*. *n* = 10 worms. (C) The ratio of *nlp-29p::GFP* to time of flight (TOF) was measured in a BIOSORT and normalized to the negative control *sta-1(RNAi)*. *n* = 95-259. Boxes are 25% percentiles above and below the median and whiskers are minimum and maximum. **P < 0.05, **P < 0.01, ***P < 0.001* versus *control(RNAi)*.

Figure 10. Working model for cuticle annular furrow regulation of stress responses. Disruption of annular furrows in the cuticle initiates signals that are transduced to *nlp-29*, *gpdh-1*, and *gst-4 via* different sets of transcription factors.

SUPPLEMENTAL FIGURES AND TABLES

Figure S1. Cuticle furrow loss activates *nlp-29p::GFP*. The ratio of *nlp-29p::GFP* to time of flight (TOF) was measured in a BIOSORT and normalized to the negative control *sta-1(RNAi)*. *n* = 78-199 worms in a trial independent of Fig. 1B. Boxes are 25% percentiles above and below the median and whiskers are minimum and maximum. ****P < 0.001* versus control *sta-1(RNAi)*. Percent acute osmotic stress resistance (OSR) was also measured. (B) Whole worm glycerol levels in N2 and *gpdh-1;gpdh-2* worms with *dpy-7(RNAi)*. *n* = 3-4 replicates for N2 and *gpdh-1;gpdh-2* worms with *dpy-7(RNAi)*. Note that N2 without *dpy-7(RNAi)* are from *n* = 4 replicates combined from two trials conducted independently and are shown for reference only. (C) Gene mRNA levels in N2 and *gpdh-1;gpdh-2* mutant worms treated with *dpy-7(RNAi)*. *n* = 4 replicates from one trial. ****P < 0.001* relative to control RNAi.

Figure S2. Heat map of RNAseq data for stress response gene expression. Conditions for comparisons are the same as in Figure 4. Sleuth analysis estimates of effect size for each comparison ('b') are provided on a $\log_2$ scale from decreased (blue) to increased (yellow) and FDR q-values are shown on a scale from high (black) to low (white). Genes are grouped by stress responses: osmolyte synthesis response (OSR), antimicrobial peptide (AMP), detoxification (DETOX), heat shock response (HSR), mitochondrial unfolded protein response (UPR^{MT}), endoplasmic reticulum unfolded protein response (UPR^{ER}), and heavy metal response (METAL).

Figure S3. Acrylamide activates *gst-4p::GFP* in *dpy-7* mutants. (A) Intestinal *gst-4p::GFP* scores for *dpy-7(e88)* worms with or without 2 mM acrylamide. Low means no visible GFP in the intestine, medium means visible GFP only in anterior or posterior intestine, and high means visible GFP throughout the intestine. (B) Images of the worms scored in A. The two images on the left were taken with the same exposure settings; the two on the right were taken with different exposures to allow visualization under both conditions. Scale bars are 100 □m.

Figure S4. Transcription factor and *gpdh* gene requirements. (A) *gst-4* mRNA levels in *skn-1a(mg570)* and N2 worms. *n* = 4 replicates from one trial. **P < 0.05* and ***P < 0.01* relative to control RNAi. (B) Survival in juglone. *P < 0.001* for *skn-1(RNAi)* in all strains. *n > 150* worms from two trials combined. (C) Elevated expression of AMP-encoding gene *nlp-29* in *dpy-10*, *dpy-7,* and *dpy-3* mutants depends on *sta-2* and *elt-3*. Ratio of *nlp-29p::GFP* to time of flight (TOF). *n* > 100 worms.

Table S1. List of real-time PCR primers

Table S2. Summary of *dpy* mutant and RNAi phenotypes

Table S3. Lists of genes with transcripts that were changed by *dpy-7*, 300 mM NaCl, and *skn-1(RNAi)* in RNAseq analysis

Table S4. Sleuth analysis of *skn-1(RNAi)* in wildtype worms

Table S5. RNAseq data for all genes differentially expressed in at least one condition

A

gene	sequence	furrows	alae	OSR	morphology phenotypes
-control					
+control					
dpy-2	T14B4.6	No	Yes	100	Dpy
dpy-3	EGAP7.1	No	Yes	100	Dpy
dpy-7	F46C8.6	No	Yes	100	Dpy, Sma
dpy-10	T14B4.7	No	Yes	98	Dpy, Sma
dpy-11	F46E10.9	Yes	No	0	Dpy, Rol
dpy-13	F30B5.1	Yes	No	0	Dpy, Sma
dpy-5	F27C1.8	Yes	No	0	Dpy
dpy-1	M01E10.2	Yes	Yes	0	Dpy
dpy-20	T22B3.1	ND	ND	0	Dpy
dpy-4	Y41E3.2	ND	ND	ND	Dpy
mlt-7	ZK430.8	ND	ND	ND	Let, Bli
bli-4	K04F10.4	ND	ND	ND	Sma, Let
klf-3	F54H5.4	ND	ND	ND	Unc, Let
mua-6	W10G6.3	ND	ND	ND	Let, Mlt
sqt-3	F23H12.4	ND	ND	ND	Rol, Lon
sqt-2	C01B12.1	Yes	Yes/No	ND	Rol, Lon
lon-1	F48E8.1	ND	ND	ND	Lon
rol-6	T01B7.7	ND	ND	ND	Lon, Rol
rol-8	ZK1290.3	ND	ND	ND	Lon, Rol

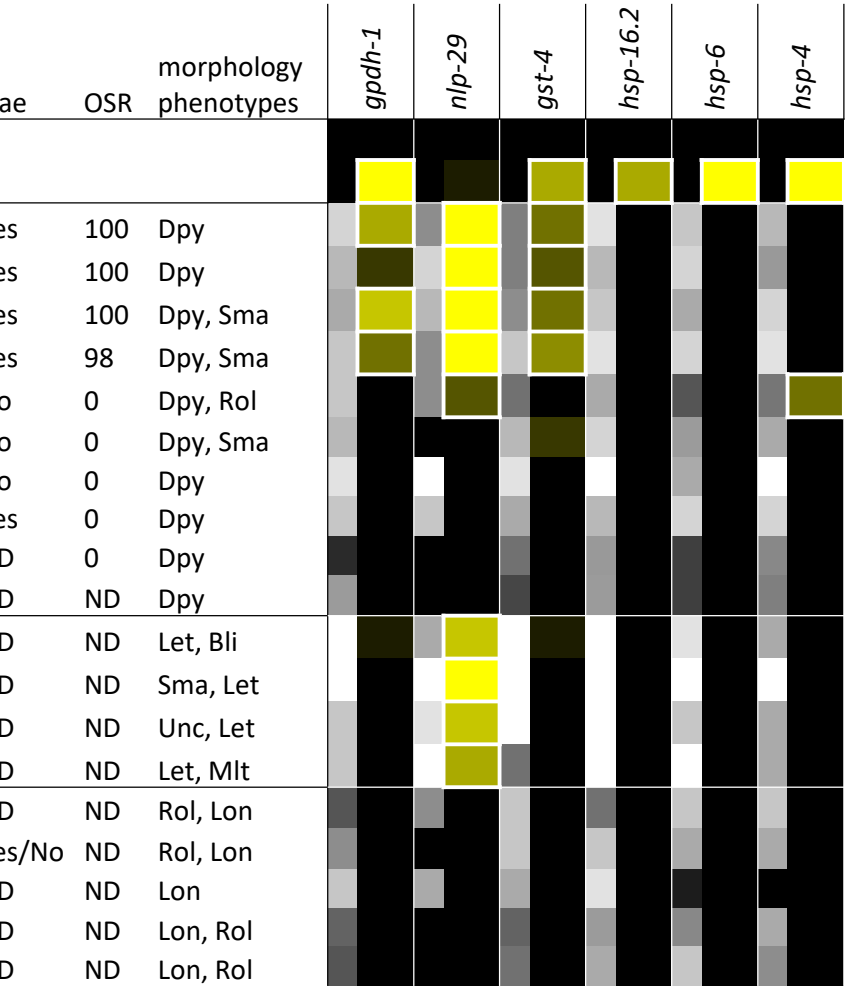

B

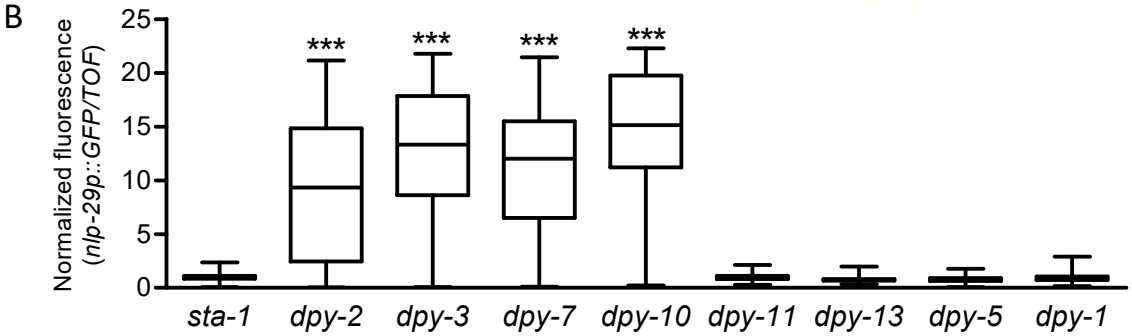

Figure 2

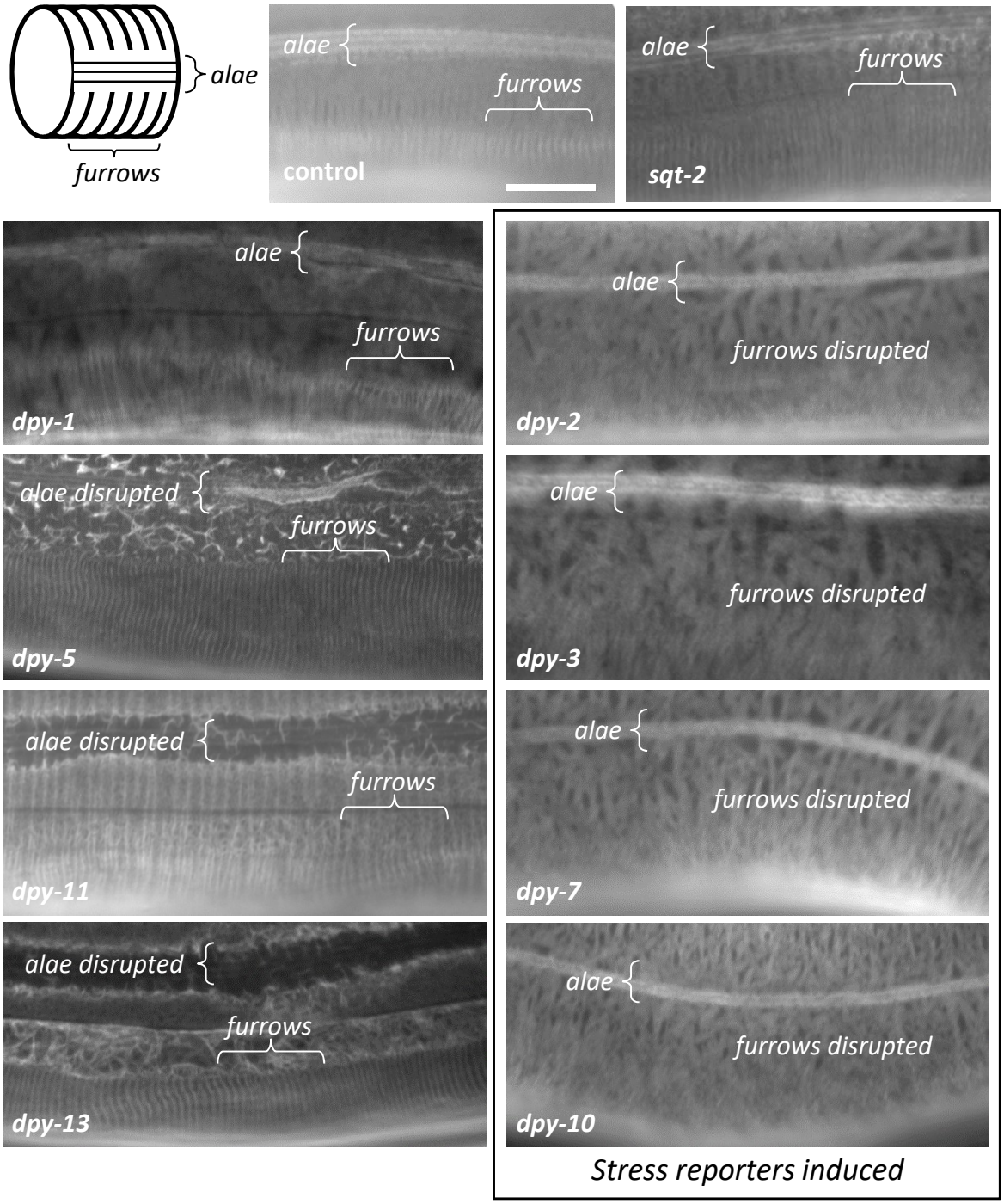
alae
furrows
alae
furrows
control
alae
furrows
sqt-2
alae
furrows
dpy-1
alae
furrows disrupted
dpy-2
alae disrupted
furrows
dpy-5
alae
furrows disrupted
dpy-3
alae disrupted
furrows
dpy-11
alae
furrows disrupted
dpy-7
alae disrupted
furrows
dpy-13
alae
furrows disrupted
dpy-10
Stress reporters induced

Figure 3

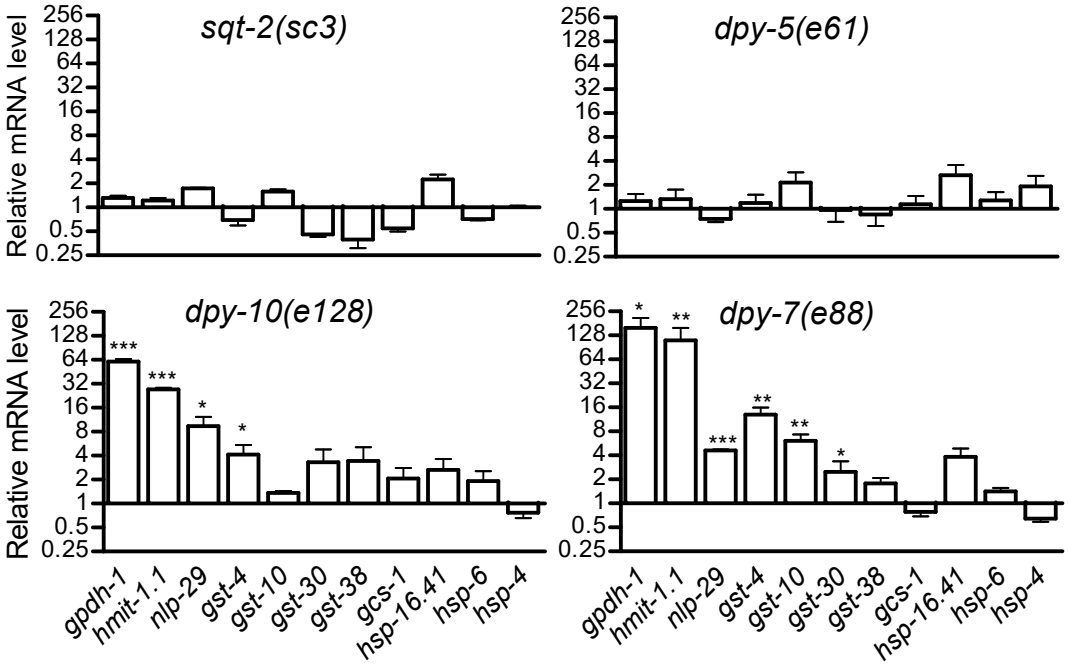
sqt-2(sc3)
dpy-5(e61)
dpy-10(e128)
dpy-7(e88)
Relative mRNA level
256
128
64
32
16
8
4
2
1
0.5
0.25
gpdh-1
hmit-1.1
nlp-29
gst-4
gst-10
gst-30
gst-38
gcs-1
hsp-16.41
hsp-6
hsp-4

Figure 4

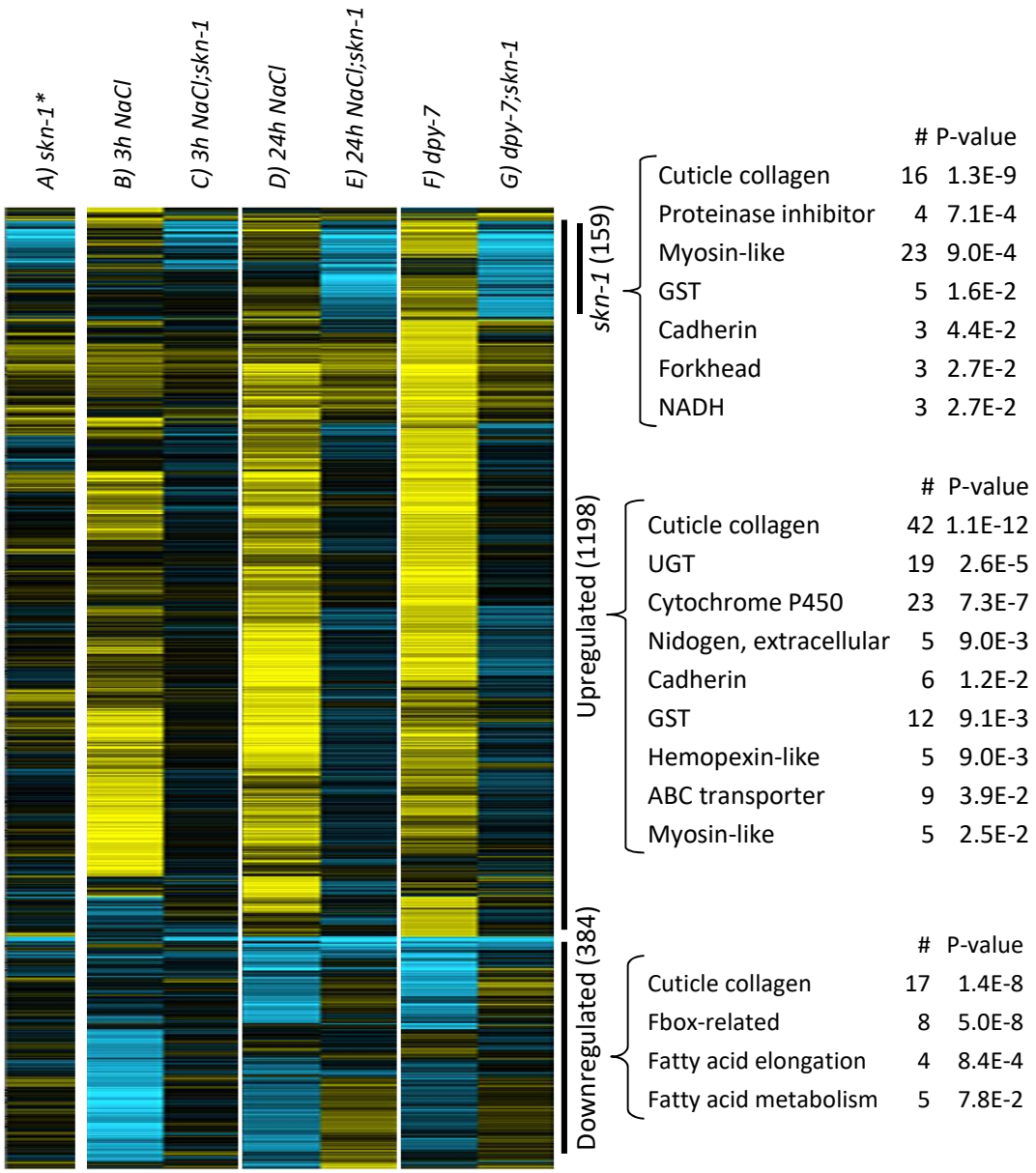

A	B	C	D	E	F	G	Treatment	Reference
1.00	0.10	0.52	0.17	0.47	0.18	0.42	*A) skn-1**	*Contol**
	1.00	-0.01	0.62	-0.14	0.42	-0.13	*B) 3h NaCl*	*3h control*
		1.00	0.09	0.44	0.06	0.39	*C) 3h NaCl;skn-1*	*3h NaCl*
			1.00	-0.06	0.77	-0.12	*D) 24h NaCl*	*24h control*
				1.00	0.07	0.70	*E) 24h NaCl;skn-1*	*24h NaCl*
					1.00	-0.10	*F) dpy-7*	*24h control*
						1.00	*G) dpy-7;skn-1*	*dpy-7*

**meta-analysis of data from GSE63075*

Figure 5

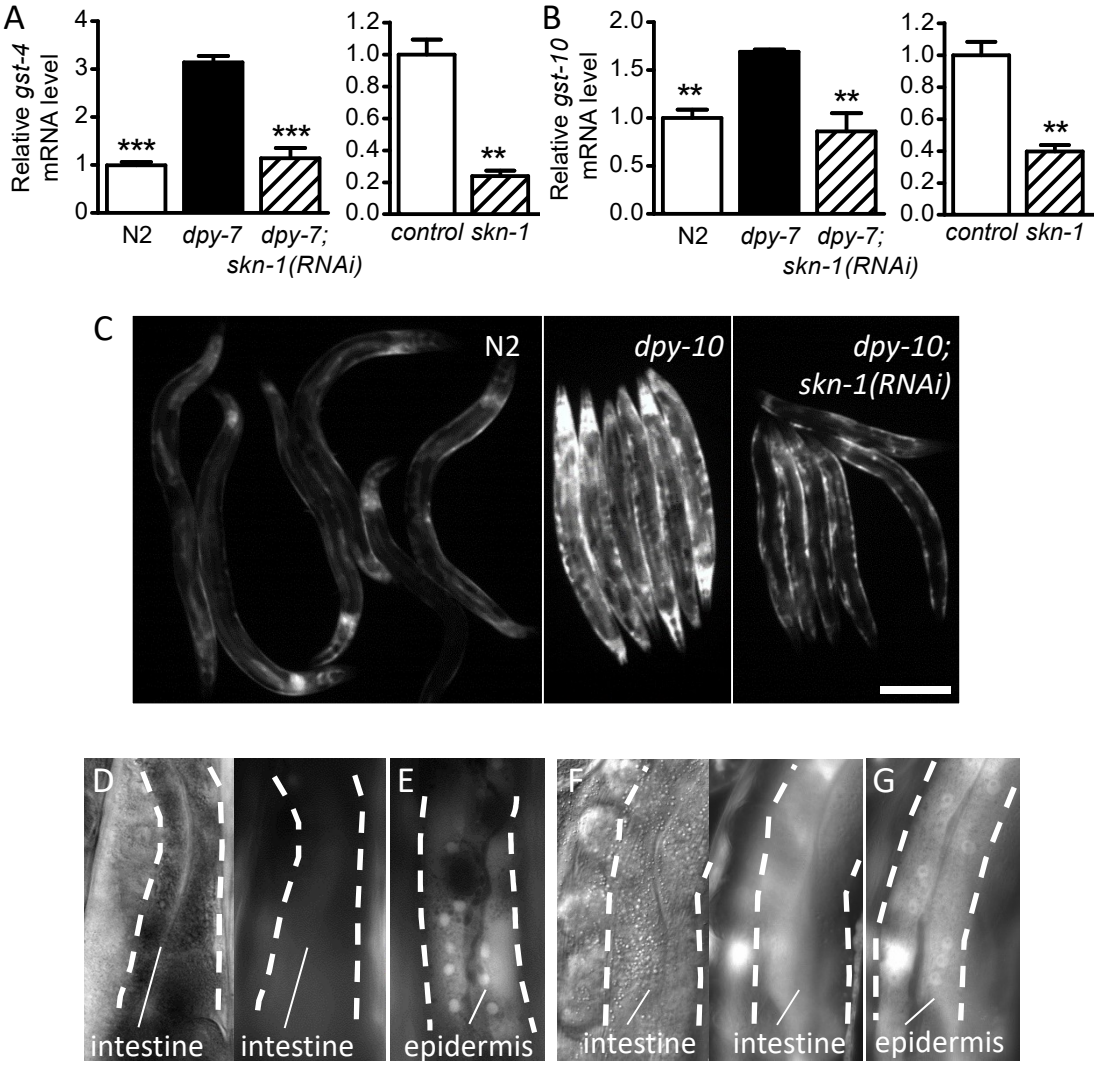
A
Relative gst-4 mRNA level
4
3
2
1
0
***
***
N2
dpy-7
dpy-7; skn-1(RNAi)
1.2
1.0
0.8
0.6
0.4
0.2
0.0
**
control
skn-1
B
Relative gst-10 mRNA level
2.0
1.5
1.0
0.5
0.0
**
**
N2
dpy-7
dpy-7; skn-1(RNAi)
1.2
1.0
0.8
0.6
0.4
0.2
0.0
**
control
skn-1
C
N2
dpy-10
dpy-10; skn-1(RNAi)
D
intestine
intestine
E
epidermis
F
intestine
intestine
G
epidermis

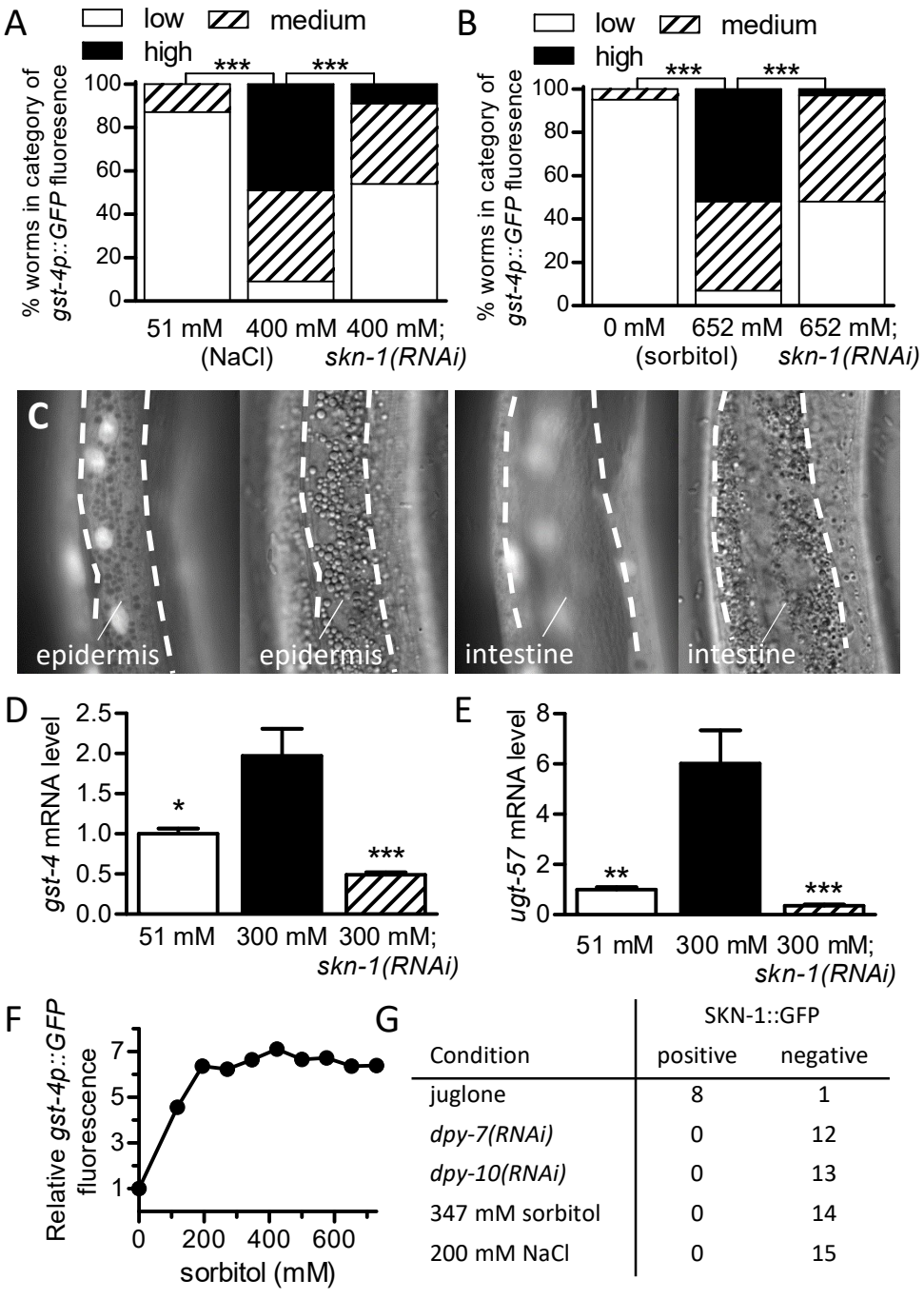

Condition	SKN-1::GFP positive	SKN-1::GFP negative
juglone	8	1
dpy-7(RNAi)	0	12
dpy-10(RNAi)	0	13
347 mM sorbitol	0	14
200 mM NaCl	0	15

Figure 7

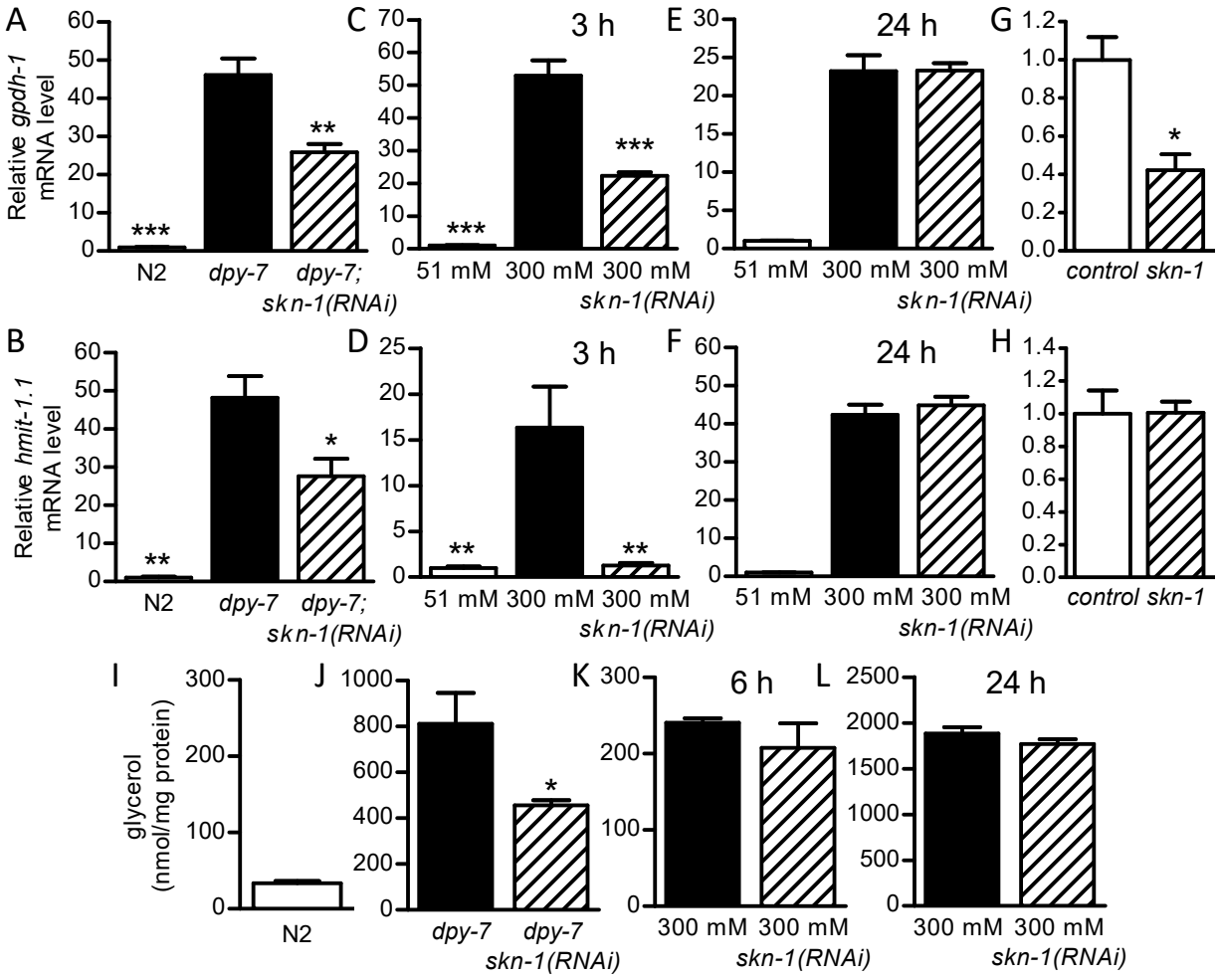
A
Relative gpdh-1 mRNA level
N2
dpy-7
dpy-7; skn-1(RNAi)
B
Relative hmit-1.1 mRNA level
C
3 h
51 mM
300 mM
300 mM skn-1(RNAi)
D
E
24 h
F
G
control
skn-1
H
I
glycerol (nmol/mg protein)
J
K
6 h
L

Figure 8

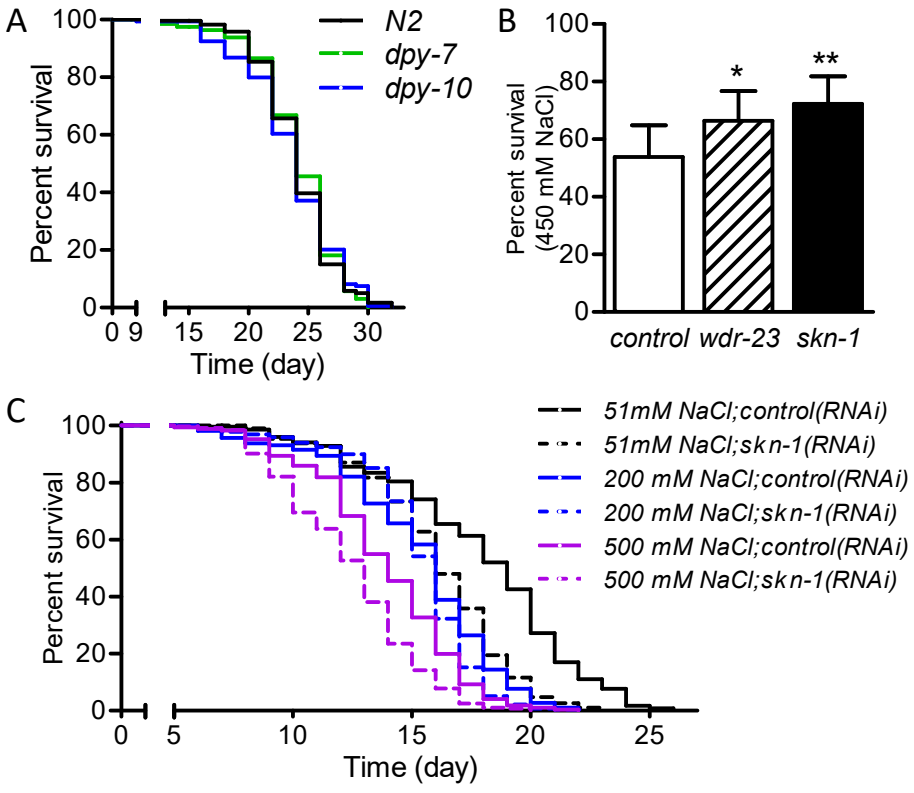
A
100
80
60
40
20
0
Percent survival
0 9 15 20 25 30
Time (day)
N2
dpy-7
dpy-10
B
100
80
60
40
20
0
Percent survival
(450 mM NaCl)
*
**
control
wdr-23
skn-1
C
100
80
60
40
20
0
Percent survival
0 5 10 15 20 25
Time (day)
51mM NaCl;control(RNAi)
51mM NaCl;skn-1(RNAi)
200 mM NaCl;control(RNAi)
200 mM NaCl;skn-1(RNAi)
500 mM NaCl;control(RNAi)
500 mM NaCl;skn-1(RNAi)

Figure 9

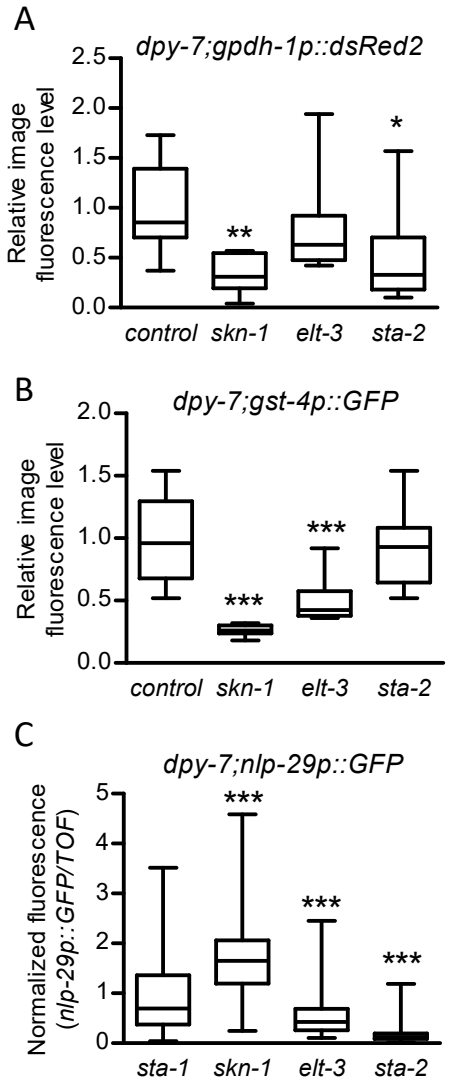
A
dpy-7;gpdh-1p::dsRed2
Relative image fluorescence level
2.5
2.0
1.5
1.0
0.5
0.0
**
*
control
skn-1
elt-3
sta-2
B
dpy-7;gst-4p::GFP
Relative image fluorescence level
2.0
1.5
1.0
0.5
0.0
***
***
control
skn-1
elt-3
sta-2
C
dpy-7;nlp-29p::GFP
Normalized fluorescence (nlp-29p::GFP/TOF)
5
4
3
2
1
0
***
***
***
sta-1
skn-1
elt-3
sta-2

Figure 10

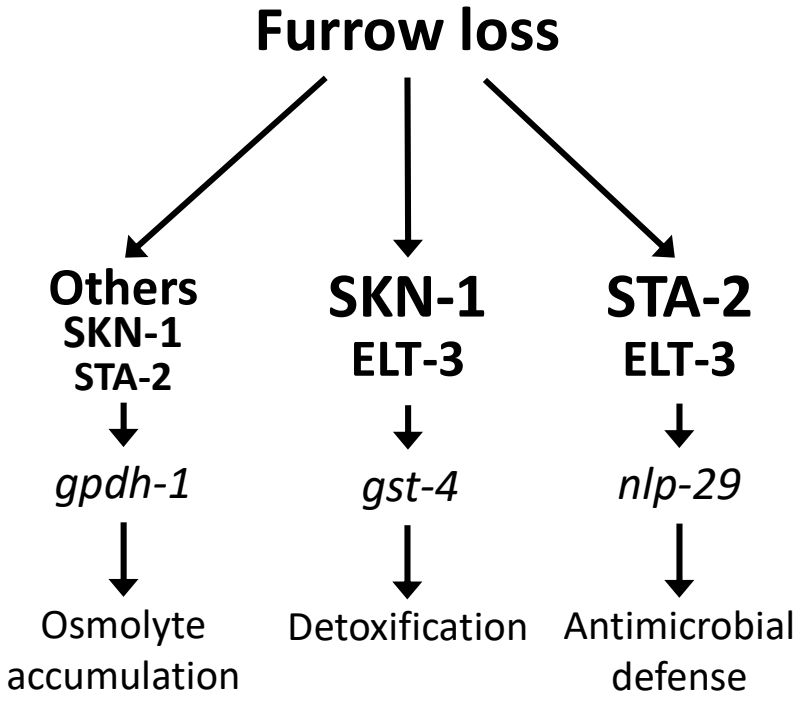
Furrow loss
Others
SKN-1
STA-2
SKN-1
ELT-3
STA-2
ELT-3
gpdh-1
gst-4
nlp-29
Osmolyte accumulation
Detoxification
Antimicrobial defense

Figure S1

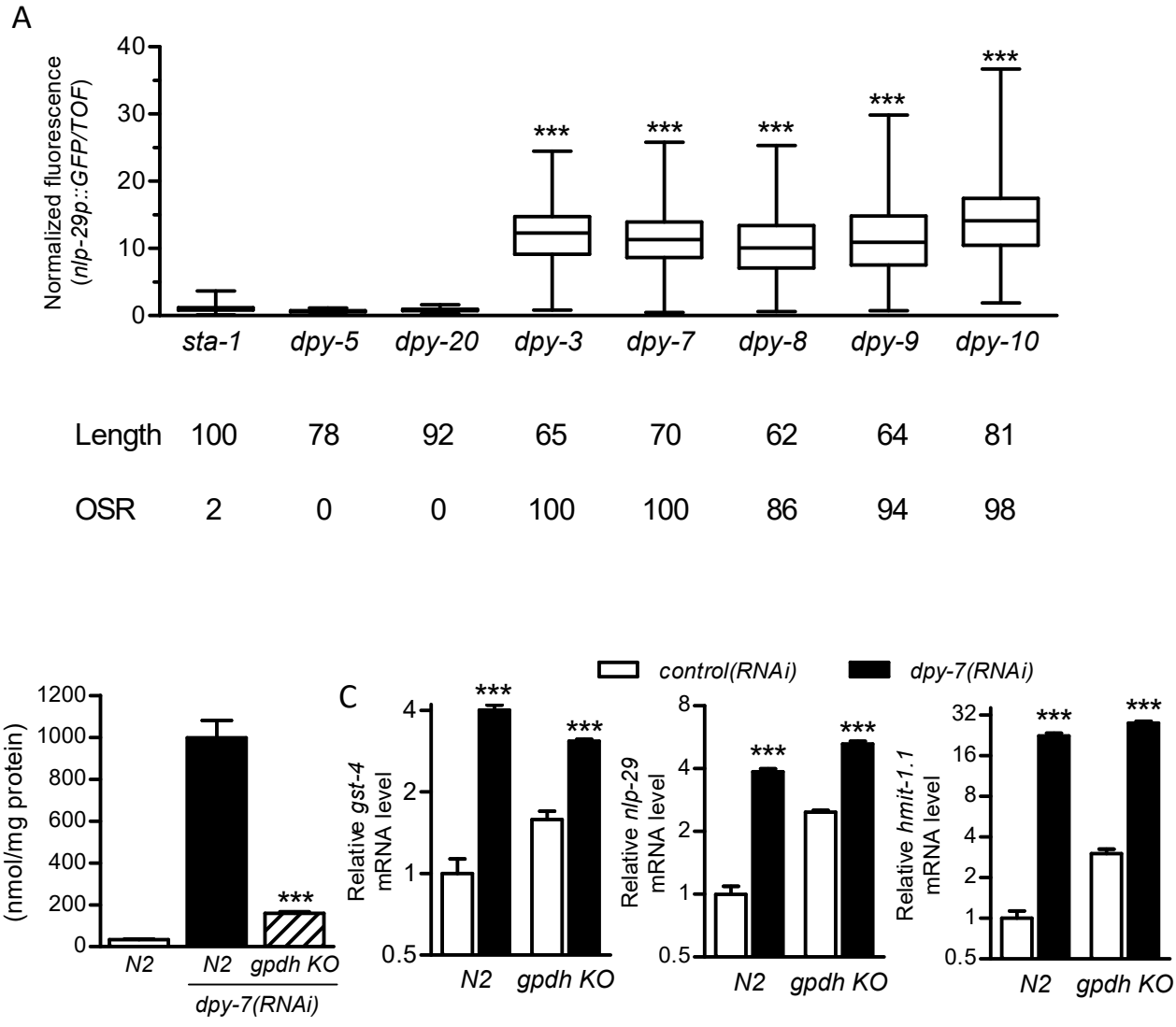
A
Normalized fluorescence (nlp-29p::GFP/TOF)
40
30
20
10
0
***
sta-1
dpy-5
dpy-20
dpy-3
dpy-7
dpy-8
dpy-9
dpy-10
Length 100 78 92 65 70 62 64 81
OSR 2 0 0 100 100 86 94 98
B
glycerol (nmol/mg protein)
1200
1000
800
600
400
200
0
N2
N2
gpdh KO
dpy-7(RNAi)
C
control(RNAi)
dpy-7(RNAi)
Relative gst-4 mRNA level
Relative nlp-29 mRNA level
Relative hmit-1.1 mRNA level
N2
gpdh KO

Figure S2

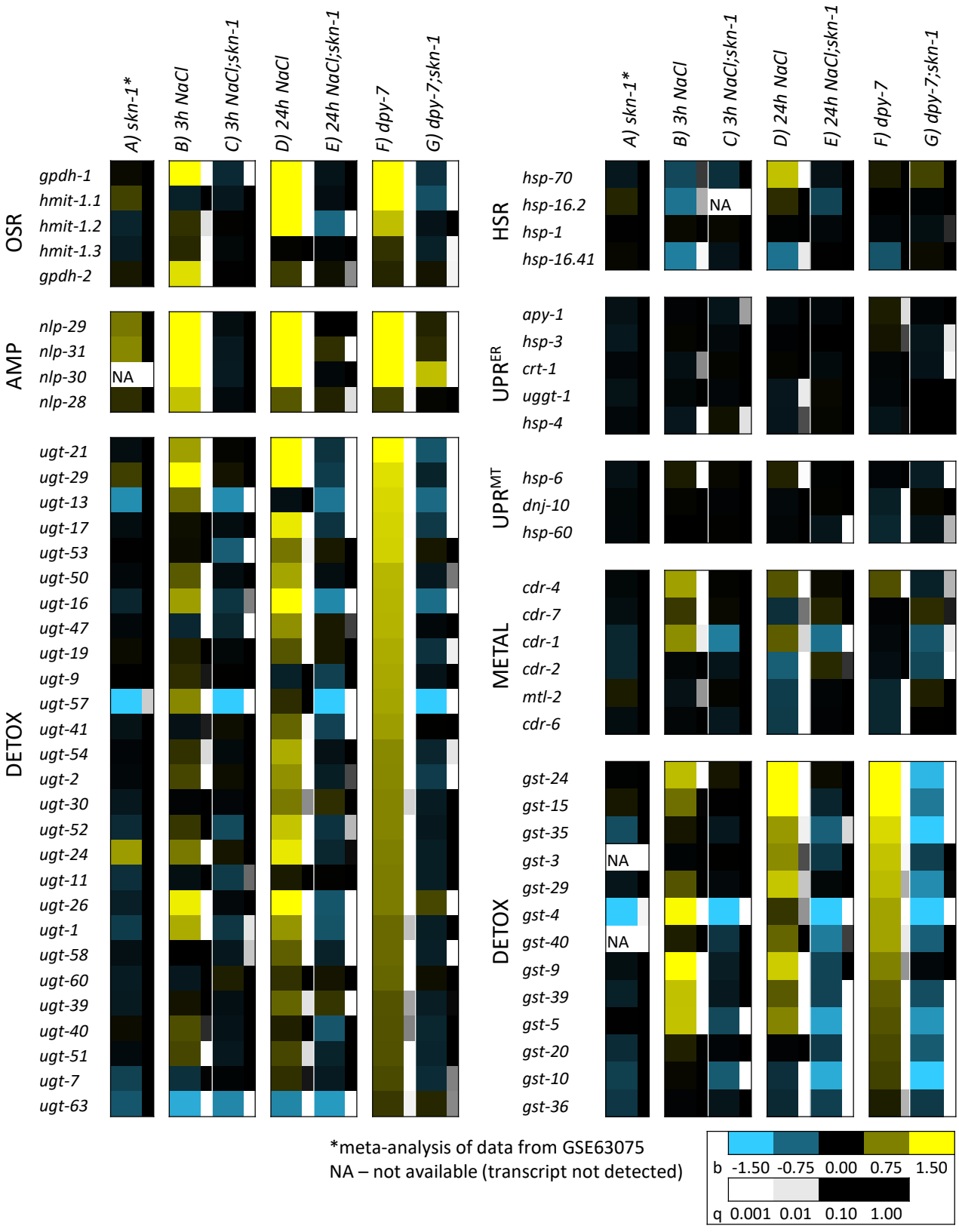

*meta-analysis of data from GSE63075
NA – not available (transcript not detected)

Figure S3

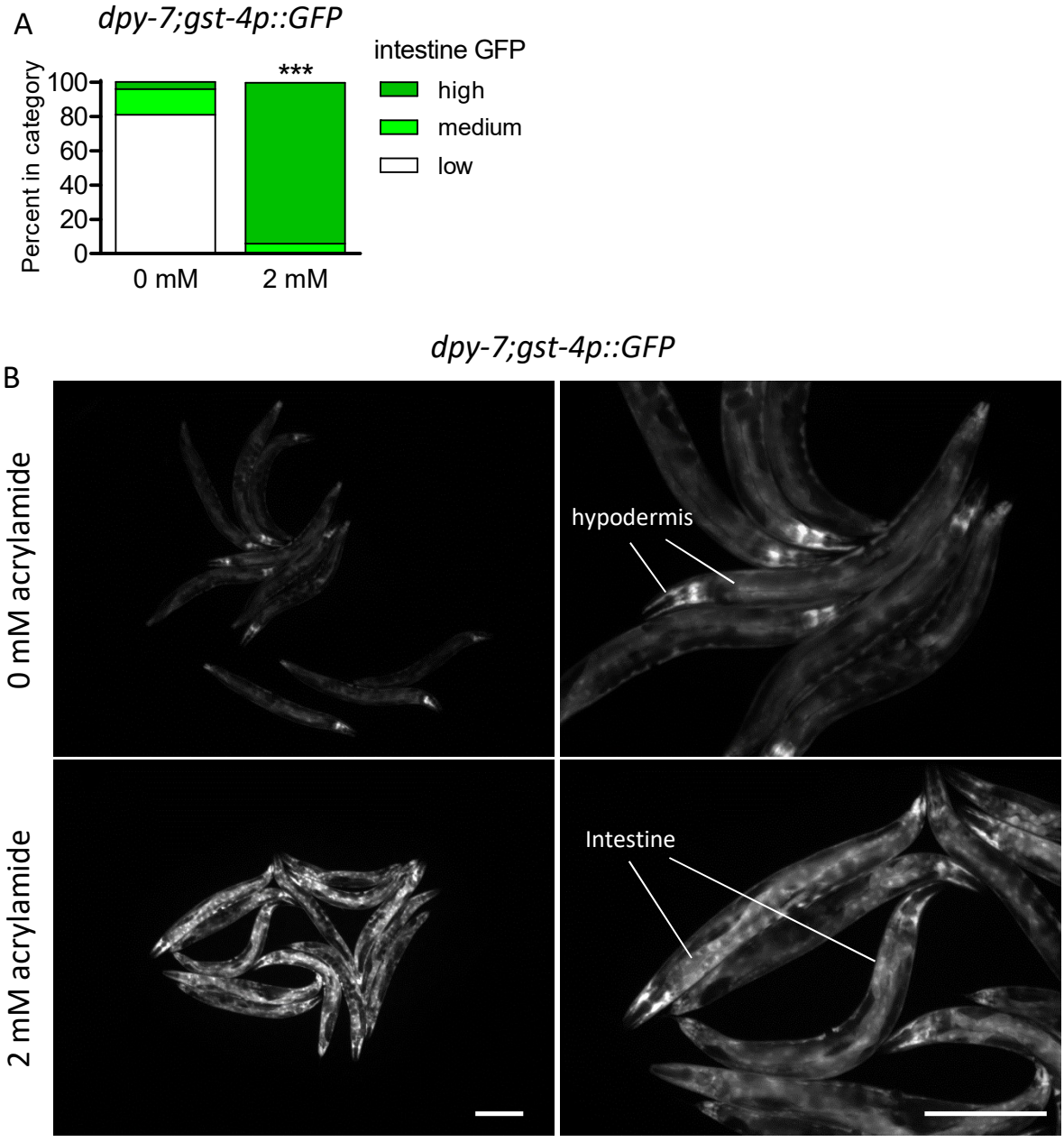
A
dpy-7;gst-4p::GFP
Percent in category
100
80
60
40
20
0
***
0 mM
2 mM
intestine GFP
high
medium
low
B
dpy-7;gst-4p::GFP
0 mM acrylamide
2 mM acrylamide
hypodermis
Intestine

Figure S4

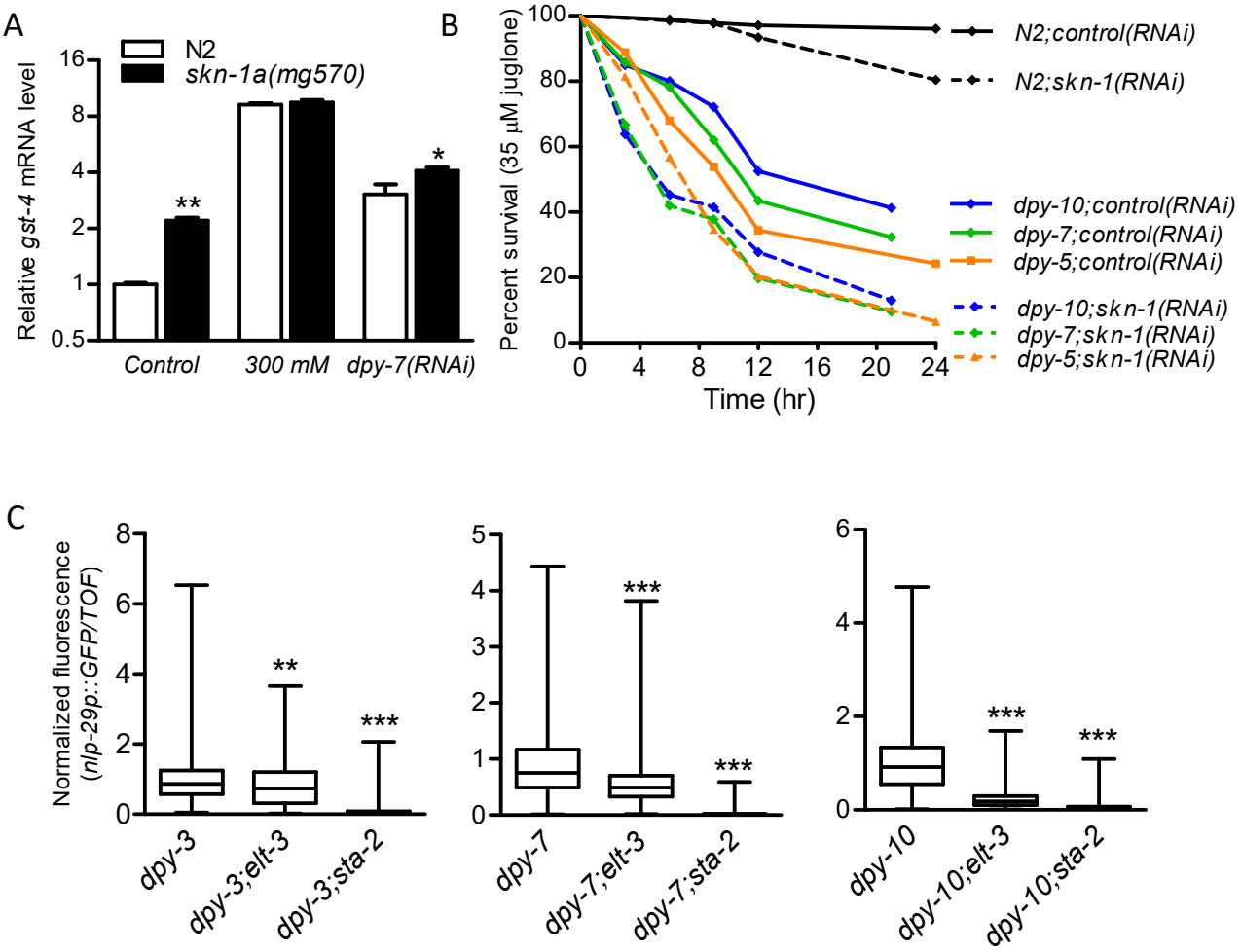
A
N2
skn-1a(mg570)
Relative gst-4 mRNA level
16
8
4
2
1
0.5
**
*
Control
300 mM
dpy-7(RNAi)
B
Percent survival (35 μM juglone)
100
80
60
40
20
0
0
4
8
12
16
20
24
Time (hr)
N2;control(RNAi)
N2;skn-1(RNAi)
dpy-10;control(RNAi)
dpy-7;control(RNAi)
dpy-5;control(RNAi)
dpy-10;skn-1(RNAi)
dpy-7;skn-1(RNAi)
dpy-5;skn-1(RNAi)
C
Normalized fluorescence
(nlp-29p::GFP/TOF)
8
6
4
2
0
**
***
dpy-3
dpy-3;elt-3
dpy-3;sta-2
5
4
3
2
1
0
***
***
dpy-7
dpy-7;elt-3
dpy-7;sta-2
6
4
2
0
***
***
dpy-10
dpy-10;elt-3
dpy-10;sta-2